

**PROJECT: EXOTIC NUCLEAR MATTER IN THE EXPLOSIVE  
STAGE OF SUPERNOVAE**  
**Raport stiintific sintetic pe intreaga perioada de executie a proiectului**

project director: F. Carstoiu

<sup>1</sup> *NINPE-HH, Division of Theoretical Physics, Bucharest-Magurele, POB MG-6, Romania*

## 1 The scientific context

The basic idea of the project was to analyze the ground state energy of ideal  $\alpha$ -matter at  $T = 0$  in the framework of variational theory of Bose quantum liquids. Calculations were executed for local  $\alpha$ - $\alpha$  potentials with positive volume integrals and two-body correlation functions obtained from the Pandharipande-Bethe equation. The energy per particle of  $\alpha$  matter could be evaluated in the cluster expansion formalism up to four-body diagrams, and using the HNC/0 and HNC/4 approximation for a Bose liquid. At low densities the two methods predict similar EOS whereas at higher densities they are sensitively different, the HNC approximation providing saturation at lower density, below the saturation value of nuclear matter. Inclusion of higher order terms in the cluster expansion of the condensate fraction is leading to a stronger depletion of the alpha condensate with the density compared to the two-body approximation prediction. In this sense five order diagrams in the Percus-Yevick approximation are evaluated in order to explore the convergence properties of the cluster expansion serie and to evaluate the contribution of small terms around the saturation point in EOS.

Renewed interest in the properties of  $\alpha$  matter is manifest in the literature especially in connection with  $\alpha$ -particle Bose-Einstein condensation (BEC) in  $\alpha$ -like nuclei (see [1] and references therein). Calculations reported in this reference are pointing to the existence of a Bose-Einstein condensate of  $\alpha$ -particles at low densities. It was also noted that with increasing density the condensate fraction is reduced such that at density corresponding to the saturation of nuclear matter ( $\rho \sim 0.04\alpha$  particles per  $\text{fm}^3$ ), the condensate fraction is reduced to roughly one half. The estimation of the condensate fraction was done in the lowest approximation, i.e. the radial distribution function (RDF) is approximated by the square of the two-body correlation function (CFN), and therefore it is less justified for higher densities. There is however an old estimation by Clark and Johnson [2] for three values around the saturation density of nuclear matter using the hypernetted chain approximation in the lowest order (HNC/0), i.e. taking into account only nodal diagrams in the infinite density expansion of the RDF. It provides a severe reduction of the condensate fraction ( $\approx 15\%$ ) compared to the lowest-order cluster expansion at the same density. On the other hand calculations of the cold  $\alpha$  matter equation of state (EOS) reported by the same authors within the HNC/0 approximation and using the soft core  $\alpha$ - $\alpha$  potential of Ali and Bodmer [3] are predicting the saturation point at a high density ( $\rho_\alpha \sim 0.085$   $\alpha$  particles per  $\text{fm}^3$ ). These benchmark calculations of the  $\alpha$  matter EOS were very recently compared to results obtained in the frame of the scalar  $\phi^5$  effective field theory with negative

quartic and positive sextic interactions, to simulate the attractive character at long distances and repulsive at short distances, and found to be in a very good agreement [4]. Though no estimations of the condensate fraction are provided for this high density saturation point, from the estimation made at lower densities, as quoted above, we expect a stronger depletion of the BEC. One is then confronted with the problem that at low densities the  $\alpha$  matter condensate is far from equilibrium, whereas at the saturation point the condensate fraction is small. It was advocated that beyond a critical density ( $\rho_\alpha \sim 0.03$  nucleons per  $\text{fm}^3$ ), due to the strong overlap of the wave-functions and the unavoidable action of the Pauli principle, a total extinction of the  $\alpha$  structure should occur [1,5]. The phenomenological  $\alpha$ - $\alpha$  potentials used in the past are systematically predicting saturation of  $\alpha$  matter at densities considerably larger than this critical Alpha-matter calculations reported in the past [1, 2] made use of  $\alpha - \alpha$  potentials with a inner repulsive part of approximately 2 fm and an outer attraction of 5 fm. These potentials, characterized by a strong or even infinite repulsive component were constructed to fit the elastic-scattering phase shifts deduced from experiment. EOS resulting from employing such potentials in the calculation of the Jackson-Feenberg (JF) expression of the energy within the paired-phonon analysis (PPA) or the HNC/0 method can be grouped in two classes. In the first class, the EOS calculated with hard-core potentials, are saturating at densities and energies close to the nuclear matter saturation point ( $\rho_\alpha \approx 0.04$ , and  $E/N \approx -11-16$  MeV). For soft-core potentials (DIPH [3] and [2]) the alpha matter almost fails to saturate. In fact a deep minimum in a very soft EOS at a high density is predicted with AB potential. However at such high densities the alpha-condensate is almost completely depleted of particles according to the variational approach. Somehow this disappointing result is conflicting with what would one expect based on the manifestation of alpha clustering in real nuclei. The clusterization of alpha particles on the surface of nuclei at densities around half the central nuclear density, as revealed by  $\alpha$ -decay or  $\alpha$ -transfer reactions or the putative dilute three- $\alpha$ s condensate in the Hoyle state of  $^{12}\text{C}$  are pointing to a higher stability of alpha matter at lower densities. It would then be important to establish if the saturation of the  $\alpha$  matter takes place below this critical density if one employs other types of potentials that incorporate more microscopic input. The aim of this Letter is to analyze the  $\alpha$  matter EOS over a wide range of densities and try to find the optimal CFN which reflects the interplay between the strong short-range and the longrange correlations that ultimately would lead to saturation. Gaining insight in the saturation properties of  $\alpha$  matter could also shed light on the condensate fraction reduction issue. In what follows the g.s. energy of an infinite system of neutral  $\alpha$ -particles interacting via two-body forces is calculated within the variational theory of Bose liquids. As input to the energy calculation we use a prescriptions for the CFN obtained by extremizing the energy functional in the two-body cluster approximation. The g.s. energy is then calculated via the cluster expansion adding the three-body and four-body correlations and with the HNC method that is more reliable in the high density sector.

Imperatives of the modern nuclear astrophysics required dedicated studies of nuclear reactions that take place in supernovae envelopes and that are the main sources of nucleosynthesis. That implied the study of some peripheral nuclear reactions that validate the ANC method

(Asymptotic Normalization Constant) which is the basic method to study in laboratory transfer and breakup reactions involving exotic (unstable) nuclei.

## 2 Scientific activity 2011

### 2.1 $\alpha - \alpha$ potentials used in scattering, $\alpha$ -cluster structure of light nuclei and alpha-matter calculations

The popular Ali-Bodmer  $\alpha - \alpha$  potential consists of a short-ranged (1.43 fm) repulsive part and a long-ranged attractive part (2.50 fm) [2]

$$v_{\alpha\alpha}(r) = 475 \exp [-(0.7r)^2] - 130 \exp [-(0.475r)^2] \quad (1)$$

This potential nicely reproduce the  $\alpha - \alpha$  elastic scattering phase-shifts for low energies. In ref.[5] an effective (not bare like AB)  $\alpha - \alpha$  potential with a soft core was proposed. This potential approximately reproduce the experimental resonant state  $E_{\text{res}}=92$  keV (see discussion below) but more important is that the relative wave function of this resonant state (and we checked this numerically)has a maximum value at 4.6 fm which is not far from value of 4 fm advocated by nuclear structure calculation of the  $^8\text{Be}$  ground state. This potential (denoted by us YS) reads

$$v_{\alpha\alpha}(r) = 50 \exp [-(0.4r)^2] - 34.101 \exp [(-(0.4r)^2)] \quad (2)$$

In a study on the differential cross sections for  $\alpha + \alpha$  elastic scattering [6] an  $l = 0$  two-body potential was constructed. It consists of an attractive part obtained by folding Gaussians  $\alpha$ -particle densities

$$\rho(r) = 32 \left( \frac{\alpha}{3\pi} \right)^{3/2} e^{-4\alpha r^2/3} \quad (3)$$

to a Yukawa-like  $N - N$  potential of range  $\mu_a$

$$v_{nn} = -85 \frac{e^{-\mu_a r}}{\mu_a r} \quad (4)$$

and additionally of a phenomenological short-range repulsive component. Thus

$$v_{\alpha\alpha}(r) = 287.5e^{-(\mu_r r)^2} - 2570.197 \frac{e^{-\mu_a r}}{\mu_a r} \{ (1 + \text{erf}(y_+) - e^{2\mu_a r} (1 + \text{erf}(y_-))) \} \quad (5)$$

where

$$y_{\pm} = \left( \frac{2\alpha}{3} \right)^{1/2} \left( r \pm 0.75 \frac{\mu_a}{\alpha} \right) \quad (6)$$

Michel and Reidemeister [7] reconsidered the old controversy between deep and shallow potentials in Heavy Ion scattering by observing e.g. that the shallow potential of Ali-Bodmer can

be approximately recovered from the deep potential of Buck et al. (BFW) [8] by a SUSY transformation. The two potentials are phase-shift equivalent, but Michel's potential is free from redundant bound states in the  $\alpha - \alpha$  system and therefore more appropriate for the  $\alpha$ -matter question. The Buck's potential reads,

$$v_{\alpha-\alpha}(r) = V_0 \exp [-(\mu r)^2] \quad (7)$$

where  $V_0 = 122.6225$  MeV,  $\mu = 0.22$  fm<sup>-2</sup>. Michel potential is identical to Buck potential for partial waves  $l > 4$ . for  $l = 0, 2$  it contains a singularity of the type  $r^{-2}$  at short distances and matches Buck's potential asymptotically.

## 2.2 Double-folding with Gogny forces

Since the potentials providing saturation at lower densities are highly schematic (infinite repulsive short-range interactions) we turn to a calculation of the bare  $\alpha - \alpha$  interaction based on the double-folding method for two ions at energies around the barrier, as input considering realistic densities of the  $\alpha$ -particle and modern effective nucleon-nucleon interactions that were not available at the moment were the above mentioned  $\alpha - \alpha$  potentials were designed.

Within the double-folding method [15] the interaction between two alpha ions is calculated as a sum of local two-body potentials  $v_{nn}$  between the nucleons from one alpha with the nucleons from the other alpha.

$$v_{\alpha\alpha}(\mathbf{r}) = \int d\mathbf{r}_1 \int d\mathbf{r}_2 \rho_{\alpha_1}(\mathbf{r}_1) \rho_{\alpha_2}(\mathbf{r}_2) v_{nn}(\rho, \mathbf{r} - \mathbf{r}_1 + \mathbf{r}_2) \quad (8)$$

The effective  $n - n$  interaction  $v_{nn}$  is taken to be dependent on density  $\rho$  of the nuclear matter where the two nucleons are embedded. It should also consist of a density independent finite-range part with preferably two ranges such that a potential similar to the Ali-Bodmer is obtained. A choice satisfying these requirement is provided by the Gogny [16]. In this paper we report results using two out of the three main parametrizations of this force, i.e. D1 [17] and the most recent one D1N [18].

In what follows we take only the direct part in the double-folding potential (8). The introduction of the exchange part of the heavy-ion interaction would lead to an unphysical deep potential for large overlaps of the two alphas. This issue was recently discussed in connection with the necessity of accounting for the incompressibility of nuclear matter in cold clustering processes [19] and extreme sub-barrier fusion [20]. In this framework a double-folding repulsive potential with a zero-range interaction is added to the direct and exchange potential such that the energy costs for overlapping two chunks of nuclear matter are payed-off. The strength of this repulsive  $\delta$ -like potential is in a simplified picture proportional to the nuclear incompressibility at the corresponding density of total overlap. We assume for the time being that the attractive exchange part of the heavy-ion potential is counteracted by the repulsive  $\delta$ -like

potential. Taking a Gaussian nuclear matter distribution inside the alpha-particle

$$\rho_\alpha(r) = 4 \left( \frac{1}{\pi b^2} \right)^{3/2} e^{-r^2/b^2} \quad (9)$$

and the oscillator parameter  $b$  corresponds to a root mean square (rms)  $1.58 \pm 0.002$  fm extracted from a Glauber analysis of experimental interaction cross sections [21].

Since the direct effective  $n - n$  force in the Gogny parametrization [22] reads:

$$v_{00}^d(\mathbf{r}_1 - \mathbf{r}_2) = \frac{1}{2} \sum_{i=1}^2 (4W_i + 2B_i - 2H_i - M_i) e^{-|\mathbf{r}_1 - \mathbf{r}_2|^2/\mu_i^2} + \frac{3}{2} t_3 \rho^\gamma \delta(\mathbf{r}_1 - \mathbf{r}_2) \quad (10)$$

Inserting the gaussian density distribution (9) in the double folding integral (9)

$$v_{\alpha\alpha}(r) = 4 \sum_{i=1}^2 (4W_i + 2B_i - 2H_i - M_i) \left( \frac{\mu_i^2}{\mu_i^2 + 2b^2} \right)^{3/2} e^{-\frac{1}{\mu_i^2 + 2b^2} r^2} + \frac{3}{2} t_3 \frac{4^{\gamma+2}}{(\gamma + 2)^{3/2} (\sqrt{\pi} b)^{3(\gamma+1)}} e^{-\frac{\gamma+2}{4b^2} r^2} \quad (11)$$

In the left panel of Fig.1 we represent the three potentials on a magnified scale around the

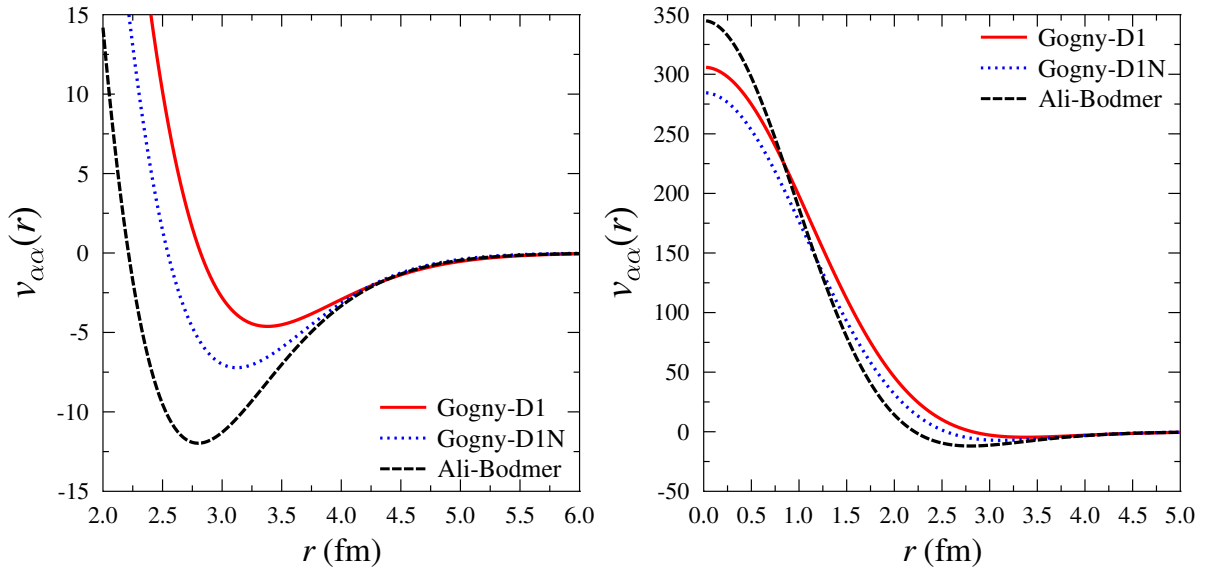


Figure 1: Different  $\alpha - \alpha$  potentials used in this paper.

minimum. The two Gogny forces display pockets that are shallower and displaced to larger radii compared to the Ali-Bodmer potential.

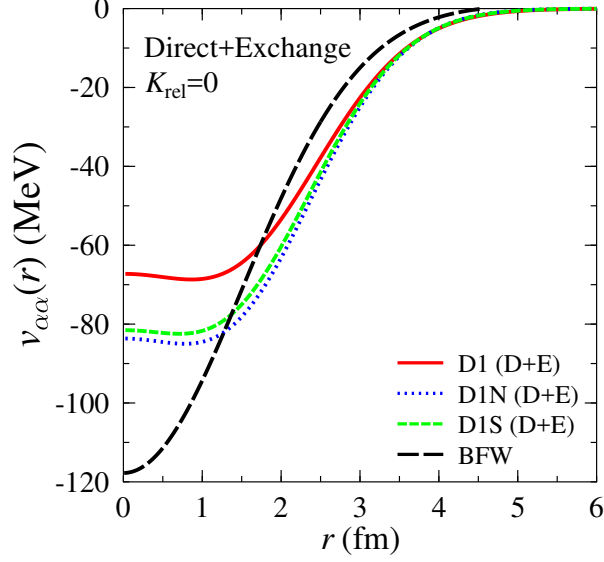


Figure 2: Direct+Exchange  $\alpha - \alpha$  potentials for BB-I, D1 and D1N.

We sketch below the derivation of the exchange part of the potential. The exchange part of the Gogny potential reads

$$v_{00}^{\text{ex}}(\mathbf{r}_1 - \mathbf{r}_2) = \frac{1}{4} \sum_{i=1}^2 (W_i + 2B_i - 2H_i - 4M_i) e^{-|\mathbf{r}_1 - \mathbf{r}_2|^2 / \mu_i^2} - \frac{3}{4} t_3 \rho^\gamma \delta(\mathbf{r}_1 - \mathbf{r}_2) \quad (12)$$

The matrix-density corresponding to the density (9) is

$$\rho_\alpha(\mathbf{r}, \mathbf{r}') = 4 \left( \frac{1}{\pi b^2} \right)^{3/2} e^{-(r_+^2 + \frac{1}{4} r_-^2) / b^2} \quad (13)$$

where

$$\mathbf{r}_+ = \frac{1}{2}(\mathbf{r} + \mathbf{r}'), \quad \mathbf{r}_- = \mathbf{r} - \mathbf{r}' \quad (14)$$

Then, in applying formula (25) from Appendix III we have

$$\rho_\alpha(\mathbf{X} + \frac{3}{2}\mathbf{R}_-, \mathbf{X} - \frac{3}{2}\mathbf{R}_-) = 4 \left( \frac{1}{\pi b^2} \right)^{3/2} e^{-(\mathbf{X} + \frac{9}{4}\mathbf{R}_-^2) / b^2} \quad (15)$$

$$\rho_\alpha(\mathbf{X} - \mathbf{R}_+ - \frac{3}{2}\mathbf{R}_-, \mathbf{X} - \mathbf{R}_+ + \frac{3}{2}\mathbf{R}_-) = 4 \left( \frac{1}{\pi b^2} \right)^{3/2} e^{-[(\mathbf{X} - \mathbf{R}_+^2) + \frac{9}{4}\mathbf{R}_-^2] / b^2} \quad (16)$$

Applying the convolution techniques we arrive at the following closed form for the non-local potential

$$v_{\alpha\alpha}^{\text{ex}}(\mathbf{R}, \mathbf{R}') = -4 \left( \frac{2}{\pi b^2} \right)^{3/2} \sum_i^2 (W_i + 2B_i - 2H_i - 4M_i) e^{-\frac{1}{2} \left( \frac{8}{\mu_i^2} + \frac{9}{b^2} \right) R_-^2} e^{-\frac{1}{2b^2} R_+^2} \quad (17)$$

Adopting the short-hand notation

$$\frac{1}{\beta_i^2} = \frac{8}{\mu_i^2} + \frac{9 + \frac{1}{4}}{b^2} \quad (18)$$

using the integral identity

$$\int d\mathbf{s} e^{-\alpha^2 s^2} e^{i\beta \mathbf{s} \cdot \mathbf{K}} = \left(\frac{\pi}{\alpha^2}\right)^{3/2} e^{-(\beta K/2\alpha)^2} \quad (19)$$

and applying the localization procedure described in Appendix III we arrive at

$$v_{\alpha\alpha}^{\text{ex}}(r) = -32 \sum_i (W_i + 2B_i - 2H_i - 4M_i) \left(\frac{\beta_i}{b}\right)^3 e^{-\frac{1}{2b^2} \left[1 - \frac{1}{4} \left(\frac{\beta_i}{b}\right)^2\right] r^2} e^{-\frac{1}{2} K^2 \beta_i^2} e^{\frac{1}{2} i \left(\frac{\beta_i}{b}\right)^2 \mathbf{K} \cdot \mathbf{r}} \quad (20)$$

Thus we have a sub-barrier branch ( $K^2 < 0$ ) and an over-barrier one ( $K^2 > 0$ ) for the real part of the local exchange potential

$$v_{\alpha\alpha}^{\text{ex}}(r) = -32 \sum_i (W_i + 2B_i - 2H_i - 4M_i) \left(\frac{\beta_i}{b}\right)^3 e^{-\frac{1}{2b^2} \left[1 - \frac{1}{4} \left(\frac{\beta_i}{b}\right)^2\right] r^2} e^{\pm \frac{1}{2} |K|^2 \beta_i^2} \\ \times \begin{cases} e^{-\frac{1}{2} \left(\frac{\beta_i}{b}\right)^2 |K| r} & \text{for } K^2 < 0 \\ \cos \left[ \frac{1}{2} \left(\frac{\beta_i}{b}\right)^2 |K| r \right] & \text{for } K^2 \geq 0 \end{cases} \quad (21)$$

The  $\alpha - \alpha$  potential when the exchange is taken into account according to the above prescription is given in Fig.2

### 2.3 Constraints on the potential due to the low-energy phase-shift data

$\alpha - \alpha$  scattering at low energies (below the first inelastic threshold) has been measured by several authors. There are no new data since 1968. S-state phase shift have been determined starting with an energy  $E_{c.m.} = 0.3$  MeV, much larger than the S-state resonance energy in  $^8\text{Be}$ . Therefore these data cannot be used to extract a potential which fits simultaneously the phase shift and the resonance energy, and therefore a compromise between the two constraints should be obtained.

### 2.4 Constraints on the potential due to the resonant state

The experimental values are  $E_{\text{res}} = 92.12 \pm 0.05$  keV,  $\Gamma_0 = 6.8 \pm 1.7$  eV [1]. We performed a systematic investigation of the renormalization required to fit the resonant state for various potentials. In table 1 we present the deep potentials, whereas in Table 2 the shallow potentials. Along with the renormalization we list the width of the resonant state. From the inspection of the last table we conclude that only the AB, BFW-supersymmetrized, and the three Gogny

$v_{\alpha\alpha}$	BFW	WS-1	WS-2	D1	D1N	D1S
$N_R$	1.007067	1.003577	0.998398	1.038707	0.898856	0.779042
$\Gamma$ (eV)	6.08	6.86	6.84	0.464413 6.57	6.19	6.04
$r_P$ (fm)	0.	0.	0.	5.02 0.	0.	0.
$V_P$ (MeV)	-123.49	-117.08	-122.36	-78.08 -32.22	-83.17	-102.22
$r_B$ (fm)	5.86	6.57	6.58	6.0	5.7	5.7
$V_B$ (MeV)	0.91825	0.78836	0.78590	5.6 0.904	0.952	0.946
				0.958		

Table 1: Renormalization and width of  $\alpha - \alpha$  potential to fit the resonant state. Deep potentials

$v_{\alpha\alpha}$	CB	AB	AB5	YS	D1S (D)	D1N (D)	D1 (D)	BB1	BB2
$N_R$	1.014808	0.946	1.307	1.005	0.616	1.591	2.444	3.998	2.099
$\Gamma$ (eV)	6.81	6.16	3.83	10.92	5.50	7.11	8.34	11.80	9.63
$r_P$ (fm)	2.9	2.82	2.07	3.82	2.7	3.1	3.40	4.10	3.7
$V_P$ (MeV)	-7.050	-9.279	-15.521	-2.843	-7.546	-9.617	-9.592	-8.413	-8.175
$r_B$ (fm)	6.50	5.77	4.39	8.47	5.6	5.90	6.3	7.2	6.7
$V_B$ (MeV)	0.7943	0.931	1.224	0.627	0.963	0.928	0.859	0.758	0.807

Table 2: Renormalization and width of  $\alpha - \alpha$  potential to fit the resonant state. Shallow potentials

$v_{\alpha\alpha}$	BFW1	BFW2	D1S	D1N	D1
$N_R$	0.994	0.948482	1.032495	0.71856	1.456354
$\Gamma$ (eV)	6.06	5.92	6.53	6.38	7.27
$r_P$ (fm)	2.80	2.80	3.0	2.8	3.10
$V_P$ (MeV)	-7.598	-7.632	-7.590	-7.13	-7.610
$r_B$ (fm)	5.8	5.8	6.0	6.2	6.2
$V_B$ (MeV)	0.924	0.925	0.897	0.8655	0.87064

Table 3: Renormalization and width of  $\alpha - \alpha$  potential to fit the resonant state. Supersymmetrized potentials

potentials are predicting widths within the experimental uncertainties. The interaction based on Brink-Boeker 2 is slightly above the experimental upper limit.

We calculated the nodeless resonant state for the shallow potentials with good values of the width. Remembering the observation we made below regarding the necessity that the wave function corresponds to a loosely bound structure of two-alpha particles that must have small values in the inner region and a maximum value around 4 fm we have additional evidence that the YS potential is not suitable to fulfill the constraints set on width and maximum. Also Ali-Bodmer, BFW-SUSY and D1S resonant wf have a minimum closer to 3 fm and therefore are conflicting with the predictions of the  $^8\text{Be}$  structure calculations. Actually only the resonant wf of D1N and D1 are displaying a maximum in the vicinity of 4 fm and simultaneously have widths in a very good agreement to the experiment. On the other hand the renormalizations of these two potentials will bring them to almost the same depths ( $\leq 10$  MeV) but with a small shift in positions. We therefore expect that potentials satisfying simultaneously the two constraints (same complex resonance energy and maximum of the radial wave function) are most likely saturating at high densities and have large binding energies.

## 2.5 The non-local exchange potential

In the double folding model, the exchange component of the optical potential can be conveniently treated starting from the DWBA matrix element of the exchange operator :

$$\hat{U}_{ex}\chi = \sum_{\alpha\beta} \langle \phi_\alpha(\mathbf{r}_1)\phi_\beta(\mathbf{r}_2) | v_{ex}(s) P_{12}^x | \phi_\alpha(\mathbf{r}_1)\phi_\beta(\mathbf{r}_2)\chi(\mathbf{R}) \rangle \quad (22)$$

where the sums runs over the single-particle wave functions of occupied states in the projectile (target) and  $\chi(\mathbf{R})$  is the wave function for relative motion. After some elementary calculation (see details in [24]), we arrive at,

$$\hat{U}_{ex}\chi = \int U_{ex}(\mathbf{R}, \mathbf{R}')\chi(\mathbf{R}')d\mathbf{R}'$$

where the kernel  $U_{ex}(\mathbf{R}, \mathbf{R}')$  is given by,

$$U_{ex}(\mathbf{R}, \mathbf{R}') = U_{ex}(\mathbf{R}^+, \mathbf{R}^-) \quad (23)$$

$$= \mu^3 v_{ex}(\mu R^-) \int \rho_1(\mathbf{X} + (1 - \frac{1}{A_1})\mu\mathbf{R}^-, \mathbf{X} - (1 - \frac{1}{A_1})\mu\mathbf{R}^- \cdot \rho_2(\mathbf{X} - \mathbf{R}^+ - (1 - \frac{1}{A_2})\mu\mathbf{R}^-, \mathbf{X} - \mathbf{R}^+ + (1 - \frac{1}{A_2})\mu\mathbf{R}^-)d\mathbf{X} \quad (24)$$

where  $\mathbf{R}^+ = (\mathbf{R} + \mathbf{R}')/2$ ,  $\mathbf{R}^- = \mathbf{R} - \mathbf{R}'$  and  $\rho(\mathbf{r}, \mathbf{r}')$  is the mixed density. The equation (23) already tells us that the range of nonlocality  $\mathbf{R}^-$  is  $\sim \mu^{-1}$ . In the case of the  $\alpha - \alpha$  interaction we have

$$U_{\alpha\alpha}^{ex}(\mathbf{R}, \mathbf{R}') = 8v_{00}^{ex}(2R^-) \int \rho_\alpha(\mathbf{X} + \frac{3}{2}\mathbf{R}^-, \mathbf{X} - \frac{3}{2}\mathbf{R}^-) \rho_\alpha(\mathbf{X} - \mathbf{R}^+ - \frac{3}{2}\mathbf{R}^-, \mathbf{X} - \mathbf{R}^+ + \frac{3}{2}\mathbf{R}^-)d\mathbf{X} \quad (25)$$

The local equivalent potential is well approximated [25] by the lowest order term of the Perey-Saxon approximation,

$$\begin{aligned}
U_L(R) &= \int e^{i\mathbf{K}\mathbf{R}^-} U_{\alpha\alpha}^{\text{ex}}(\mathbf{R} + \frac{1}{2}\mathbf{R}^-, \mathbf{R}^-) d\mathbf{R}^- \\
&= 4\pi \int \rho_\alpha(X) \rho_\alpha(|\mathbf{R} - \mathbf{X}|) d\mathbf{X} \\
&\times \int v_{00}^{\text{ex}}(s) \hat{j}_1(\hat{k}_1(X) \frac{3}{4}s) \cdot \hat{j}_1(\hat{k}_2(|\mathbf{R} - \mathbf{X}|) \frac{3}{4}s) j_0(K(R)s/2) s^2 ds \quad (26)
\end{aligned}$$

where  $K(R)$  is the usual WKB local momentum for the relative motion,

$$K^2(R) = \frac{2\mu}{\hbar^2} (E_{c.m.} - U_D(R) - U_L(R)) \quad (27)$$

where where  $U_D$  is the direct term including the nuclear and Coulomb potentials. Truly speaking, the classical momentum is defined only for energies where  $K^2(R) \geq 0$ . At underbarrier energies,  $K(R)$  is imaginary in the region  $R_1 < R < R_2$ , where  $R_{1,2}$  are the classical turning points of the total potential, and the Bessel function  $j_0$  above should be replaced by  $j_0(ix) = \sinh(|x|)/|x|$ .

## References

- [1] M. T. Johnson and J. W. Clark, *Variational Theory of Ideal Alpha Matter*, Kinam, **2**, 3 (1979).
- [2] G. P. Mueller and J.W. Clark, Nucl. Phys.**A155**, 561 (1970).
- [3] P. Darriulat, G. Igo, H. G. Pugh and H. D. Holmgren, Phys. Rev.**137**, B315 (1965).
- [4] S. Ali and A. R. Bodmer, Nucl. Phys.**A80**, 99 (1966).
- [5] T. Yamada and P. Schuck, Phys. Rev.**C69**, 024309 (2004).
- [6] W. S. Chien and R. E. Brown, Phys. Rev.**C10**, 1767 (1974).
- [7] F. Michel and Reidemeister, J. Phys.**G11**, 835(1985).
- [8] Buck, Friedrich and Wheatley, Nucl. Phys.**A275**, 246(1977)
- [9] V. G. Neudatchin, V. I. Kukulin, V. L. Korotkikh and V. P. Korennoy, Phys. Lett.**B34**, 581 (1971)
- [10] V. I. Kukulin, V. G. Neudatchin and Yu. F. Smirnov, Nucl. Phys.**A245**, 429 (1975)

- [11] L. Marquez, Phys. Rev. **C28**, 2525 (1983).
- [12] H. Takemoto et al., Phys. Rev. **C69**, 035802 (2004).
- [13] K. A. Gridnev et al., Int.J.Mod.Phys.E **14**, 635 (2005).
- [14] E. Feenberg, Ann. Phys.(N.Y.)**84**, 128 (1974).
- [15] F. Carstoiu and R.J. Lombard , Ann. Phys.(N.Y.)**217**, 279 (1992)
- [16] D. Gogny, in Proc. Int. Conf. on Nuclear Physics, eds. J. De Boer and H. Mang (North-Holland, Amsterdam, 1973)
- [17] J. Dechargé and D. Gogny, Phys. Rev. **C21**, 1568 (1980).
- [18] F. Chappert, M. Girod and S. Hilaire, Phys. Lett. **B668**, 420 (2008).
- [19] D.S.Delion, A.Sandulescu, Ş.Mişicu and F.Carstoiu and W.Greiner, Phys. Rev. **C64** 041303 (2001).
- [20] Ş. Mişicu and H.Esbensen, Phys. Rev. Lett. **91**, no.11, 112701 (2006).
- [21] J. S. Al-Khalili, J. A. Tostevin and I. J. Thompson, Phys. Rev. **C54**, 1843 (1996).
- [22] Ş. Mişicu and F. Carstoiu, Phys. Lett. **B682**, 33 (2009).
- [23] J. Benn, E. B. Dally, H. H. Müller, R. E. Pixley, H. H. Staub and H. Winkler, Phys.Lett. **20**, 43 (1966).
- [24] F. Carstoiu and M. Lassaut, Nucl. Phys. **A597**, 269 (1996).
- [25] R. E. Peierls and N. Vinh Mau, Nucl. Phys. **A343**, 1 (1980).

### 3 Scientific activity 2012

#### 3.1 A new method to remove redundant states

We describe bellow a new method to remove Pauli forbidden states using supersymmetric transformations.

### 3.2 Notations

We consider the Schrödinger equation for the  $\ell$ -wave

$$\left( \frac{d^2}{dr^2} + \frac{2\mu}{\hbar^2}(E - V(r)) - \frac{\ell(\ell + 1)}{r^2} \right) \psi_\ell(E, r) = 0 \quad (28)$$

where  $\psi_\ell(E, r)$  is called the regular solution which is uniquely defined, as usual [28, 29], by the Cauchy condition  $\lim_{r \rightarrow 0} \psi_\ell(E, r)r^{-\ell-1} = 1$ . It behaves for positive values of  $E$  as  $\psi_\ell \propto \sin(kr - \ell\pi/2 + \delta(\ell, k))$  when  $r \rightarrow \infty$  ( $k = \sqrt{2\mu E/\hbar^2}$ ), provided that  $V(r)$  satisfies the integrability condition [29]

$$\int_b^{+\infty} |V(r)|dr < \infty, \quad b > 0, \quad \int_0^\infty r|V(r)|dr < \infty \quad (29)$$

Here, the  $\delta(\ell, k)$ 's are the phase shifts. In all equations  $\mu$  denotes the reduced mass of the system and  $E$  the c.m. energy.

When the potential possesses bound states labeled  $E_0 < E_1 < \dots < E_N \leq 0$  (the number of which is finite when the potential satisfies the integrability condition Eq.(29) these latter can be removed thanks to the procedure introduced by Baye.

### 3.3 Phase-equivalent potentials

Here we give the equations allowing to obtain directly, from the bound state wave functions for the  $0s$  and  $1s$  states, the wanted potential for  $\alpha$ -matter.

Let us recall the remove of the ground state. Let be  $\psi_\ell(E_0, r)$  the ground state wave function normalized according to the above Cauchy condition. We introduce the reduced potential  $v(r) = 2\mu V(r)/\hbar^2$ . The phase-equivalent potential  $v^{(1)}(r)$ , obtained by Baye with the ground state removed, reads:

$$v^{(1)}(r) = v(r) - 2 \frac{d^2}{dr^2} \ln \int_0^r dt \psi_\ell(E_0, t)^2 \quad (30)$$

The corresponding regular solution for  $v^{(1)}$  is

$$\psi_\ell^{(1)}(E, r) = \psi_\ell(E, r) - \psi_\ell(E_0, r) \frac{\int_0^r dt \psi_\ell(E, t) \psi_\ell(E_0, t)}{\int_0^r dt \psi_\ell(E_0, t)^2} \quad (31)$$

The potential  $v^{(1)}(r)$  behaves at the vicinity of  $r = 0$  like  $2(2\ell + 3)/r^2$ . This is due to its definition Eq.(30) taking into account that  $\psi_\ell(E_0, r) \simeq r^{\ell+1}$  at the vicinity of zero.

Now we want to remove the next bound state  $E_1$ . The new potential and regular solutions are defined respectively by:

$$v^{(2)}(r) = v^{(1)}(r) - 2 \frac{d^2}{dr^2} \ln \int_0^r dt \psi_\ell^{(1)}(E_1, t)^2 \quad (32)$$

and

$$\psi_\ell^{(2)}(E, r) = \psi_\ell^{(1)}(E, r) - \psi_\ell^{(1)}(E_1, r) \frac{\int_0^r dt \psi_\ell^{(1)}(E, t) \psi_\ell^{(1)}(E_1, t)}{\int_0^r dt \psi_\ell^{(1)}(E_1, t)^2}. \quad (33)$$

We evaluate  $\psi_\ell^{(1)}(E_1, r)^2$  from the original wave function  $\psi_\ell$ . Thanks to Eq.(31) we have

$$\psi_\ell^{(1)}(E_1, r)^2 = \psi_\ell(E_1, r)^2 - \frac{d}{dr} \left[ \frac{(\int_0^r dt \psi_\ell(E_1, t) \psi_\ell(E_0, t))^2}{\int_0^r dt \psi_\ell(E_0, t)^2} \right] \quad (34)$$

so that

$$\int_0^r dt \psi_\ell^{(1)}(E_1, t)^2 = \int_0^r dt \psi_\ell(E_1, t)^2 - \frac{(\int_0^r dt \psi_\ell(E_1, t) \psi_\ell(E_0, t))^2}{\int_0^r dt \psi_\ell(E_0, t)^2} \quad (35)$$

Now, taking into account the equations (30,32) we have

$$v^{(2)}(r) = v(r) - 2 \frac{d^2}{dr^2} \ln \det(M(r)) \quad (36)$$

where  $M$  is the  $2 \times 2$  matrix

$$M = \begin{bmatrix} L_{E_0, E_0}(\ell, r) & L_{E_0, E_1}(\ell, r) \\ L_{E_1, E_0}(\ell, r) & L_{E_1, E_1}(\ell, r) \end{bmatrix} \quad (37)$$

with

$$L_{E_i, E_j}(\ell, r) = L_{E_j, E_i}(\ell, r) = \int_0^r dt \psi_\ell(E_i, t) \psi_\ell(E_j, t). \quad (38)$$

Clearly the determinant of the matrix  $M$  behaves like  $r^{4\ell+10}$  at the vicinity of zero and the resulting potential has a singularity  $(8\ell + 20)/r^2$  at the vicinity of zero.

On the other hand, the regular solution can be also put on a compact form according to what made in [30] Appendix B. Indeed, we first note that the product  $\psi_\ell^{(1)}(E, r) \psi_\ell^{(1)}(E_1, r)$  can be written as

$$\psi_\ell^{(1)}(E, r) \psi_\ell^{(1)}(E_1, r) = \psi_\ell(E, r) \psi_\ell(E_1, r) - \frac{d}{dr} \left[ \frac{\int_0^r dt \psi_\ell(E, t) \psi_\ell(E_0, t) \int_0^r dt \psi_\ell(E_1, t) \psi_\ell(E_0, t)}{\int_0^r dt \psi_\ell(E_0, t)^2} \right] \quad (39)$$

The latter equality is used to calculate  $\int_0^r dt \psi_\ell^{(1)}(E, t) \psi_\ell^{(1)}(E_1, t)$  required in Eq.(33). Taking into account the equation (35) we obtain, after some algebra

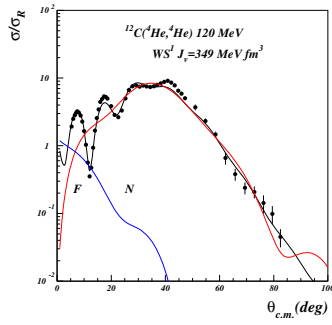
$$\psi_\ell^{(2)}(E, r) = \frac{\det(\tilde{M}(r))}{\det(M(r))} \quad (40)$$

where we have defined

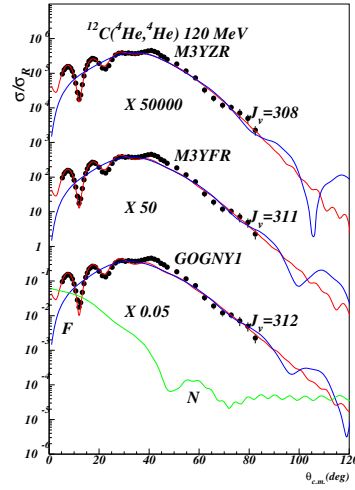
$$\tilde{M} = \begin{bmatrix} \psi_\ell(E, r) & L_{E, E_0}(\ell, r) & L_{E, E_1}(\ell, r) \\ \psi_\ell(E_0, r) & L_{E_0, E_0}(\ell, r) & L_{E_0, E_1}(\ell, r) \\ \psi_\ell(E_1, r) & L_{E_1, E_0}(\ell, r) & L_{E_1, E_1}(\ell, r) \end{bmatrix} \quad (41)$$

### 3.4 Test of effective interactions on $\alpha$ -nucleus scattering

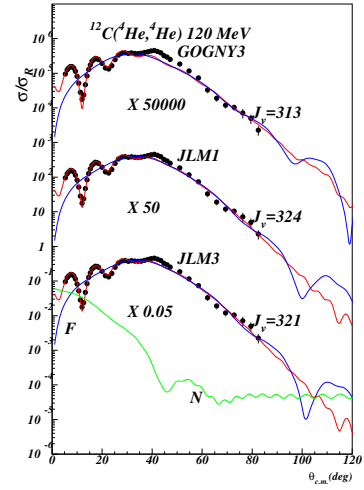
We first tested the ability of well known effective interactions to describe correctly the  $\alpha$ -nucleus scattering at various energies. We concentrate mainly on  $4N$  targets with known  $\alpha$  cluster structure in the ground state or low excited states. The next figure contains examples of  $\alpha$ - $^{12}\text{C}$  scattering at high energies where rainbow phenomenon is evident. We were mainly interested to test the Gogny interaction in scattering.



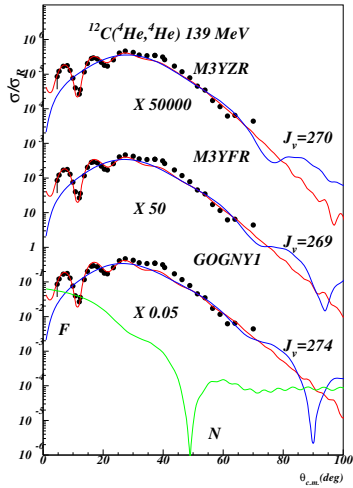
(a)



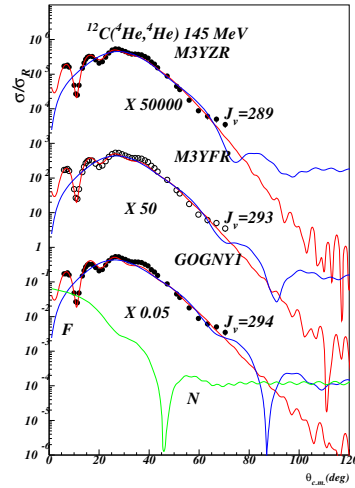
(b)



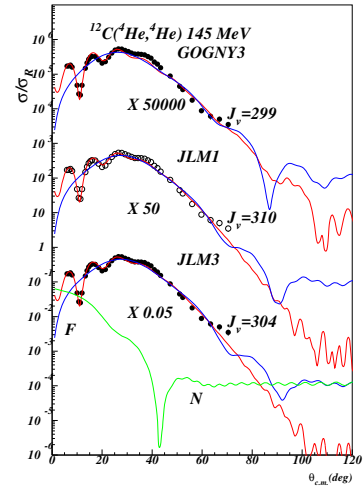
(c)



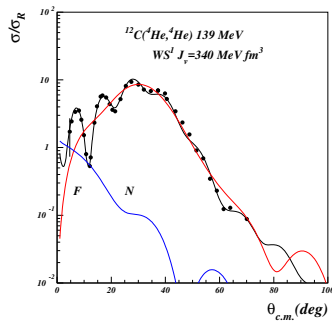
(d)



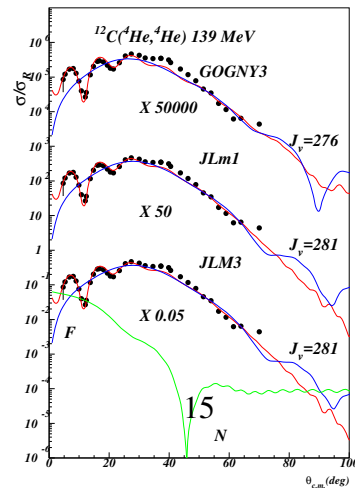
(e)



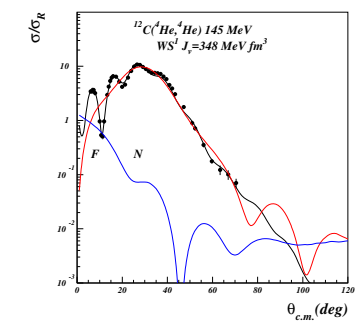
(f)



(g)



(h)



(i)

### 3.5 Constraints on the potential due to the low-energy phase-shift data

$\alpha$ - $\alpha$  scattering at low energies (below the first inelastic threshold) has been measured by several authors. There are no new data since 1968. S-state phase shift have been determined starting with an energy  $E_{c.m.}=0.3$  MeV, much larger than the S-state resonance energy in  ${}^8\text{Be}$ . Therefore these data cannot be used to determine uniquely a potential which fits simultaneously the phase shift and the resonance energy, and therefore a compromise between the two constraints should be obtained. We adopted a slight renormalization of the strengths and ranges of potentials. See Fig.4.

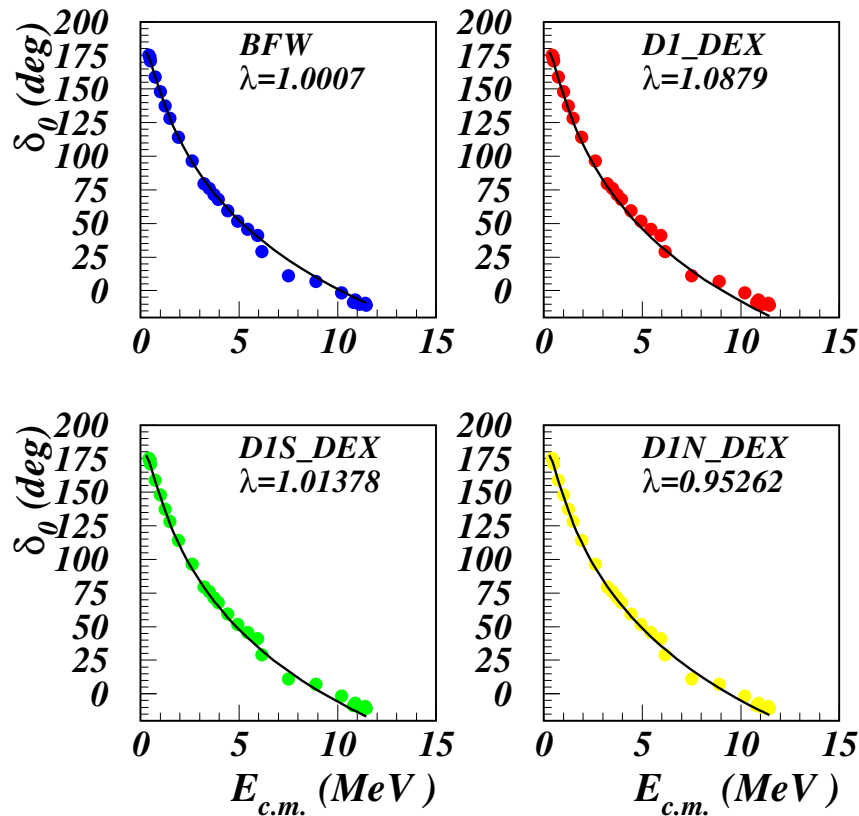


Figure 4: Low energy S-state phase shifts calculated with renormalized  $\alpha - \alpha$  potentials. The calculations are based on the Calogero equation. Experimental data are plotted with dots. Renormalization constants are denoted by  $\lambda$ .

### 3.6 Constraints on the potential due to the resonant state

The experimental values are  $E_{\text{res}} = 92.12 \pm 0.05$  keV,  $\Gamma_0 = 6.8 \pm 1.7$  eV [1]. We performed a systematic investigation of the renormalization required to fit the resonant state for various potentials. While the resonant energy is close to the experimental value for all interactions, only the BFW and Gogny D1 reproduce correctly the experimental width, see Fig.5 . However the D1S and D1N parametrizations of the Gogny interaction predict widths within the experimental error barr.

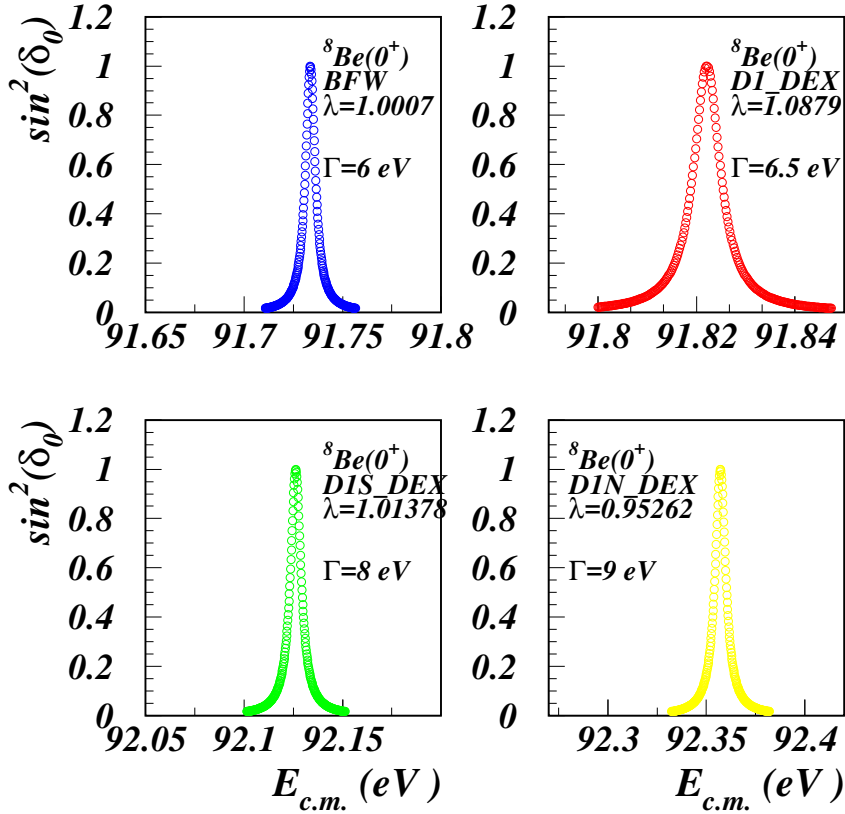


Figure 5: The  $0^+$  resonance in  ${}^8\text{Be}$  calculated with renormalized effective interactions ( $\lambda$ ). Only the BFW and Gogny D1 interactions reproduce correctly the experimental width of 6 eV.

### 3.7 Supersymmetric partners of the bare interactions

Once we have obtained the bare interactions by folding including the local equivalent of the knock on exchange kernel we calculate the wave functions for the redundant 0s and 1S states and then we calculate the potential free of redundant states by applying the supersymmetry transformation as outlined in the preceding section. The result is depicted in Fig.6.

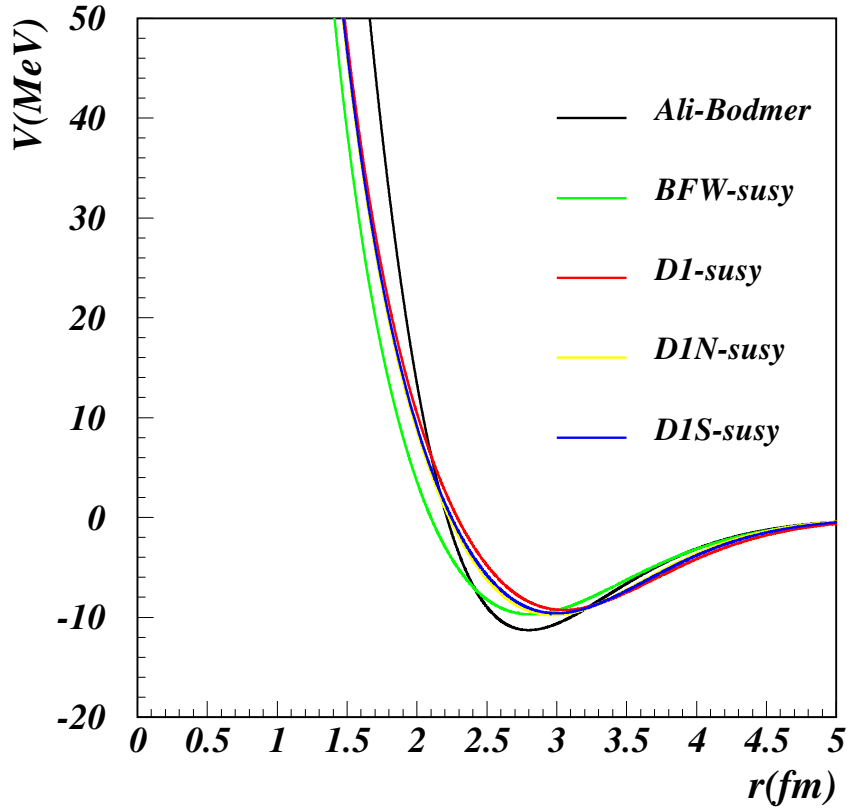


Figure 6: The supersymmetric partners of the renormalized bare BFW and Gogny interactions are compared with Ali-Bodmer phenomenological interaction. We have checked that original phase shifts and the  $0^+$  resonance properties are conserved

### 3.8 Gaussian expansion of the SUSY potentials

In order to facilitate the calculation for  $\alpha$ -matter we expand the SUSY potentials in gaussian formfactors, similar to the Ali-Bodmer interaction,

$$V_{fit}(r) = V_r e^{-(\mu_r r)^2} - V_a e^{-(\mu_a r)^2} \quad (42)$$

with  $V_r, \mu_r, V_a, \mu_a$  fitting parameters. Since it is impossible to obtain meaningful parameters in the whole radial range, we concentrate the fit in the relevant  $r = (1.5, 10)$  fm. The result is given in the following table,

Int	$V_r(\text{MeV})$	$\mu_r(\text{fm}^{-1})$	$V_a(\text{MeV})$	$\mu_a(\text{fm}^{-1})$
BFW	254.8000031	0.6470000	101.9716263	0.4600000
D1	255.8999939	0.6049346	103.6447830	0.4370000
D1N	265.0000000	0.6266215	102.5655823	0.4459522
D1S	262.0000000	0.6194427	103.4447250	0.4437624

Table 4: Parameters for the fitted SUSY potentials

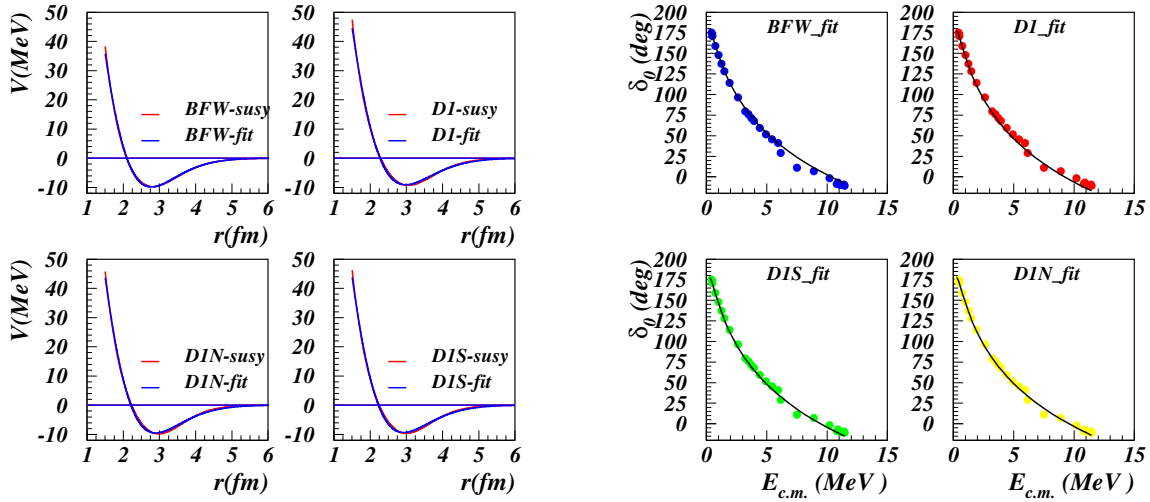


Figure 7: Comparison of the original Susy potentials and the Gaussian expansion

Figure 8: Check of the phase-shift calculated with the fitted Susy-potential

### 3.9 Five-body diagrams in the Percus Yevick approximation

For the five-body contribution to the g.s. energy the application of the  $\delta$ -folding technique leads to the following expressions for the diagrams needed in the PY approximation

$$\mathcal{E}_5^{(0)} = \frac{1}{2} \begin{array}{c} \bullet \\ \diagup \quad \diagdown \\ \bullet \quad \bullet \\ \diagdown \quad \diagup \\ \circ \cdots \circ \\ \bullet \\ \diagup \quad \diagdown \\ \bullet \quad \bullet \\ \diagdown \quad \diagup \\ \circ \quad \circ \end{array} = \frac{\rho^4}{2} \int d\mathbf{R} F(R) [h * [h * [h * h]]](R) \quad (43)$$

$$\mathcal{E}_5^{(1)} = \begin{array}{c} \bullet \\ \diagup \quad \diagdown \\ \bullet \quad \bullet \\ \diagdown \quad \diagup \\ \circ \cdots \circ \\ \bullet \\ \diagup \quad \diagdown \\ \bullet \quad \bullet \\ \diagdown \quad \diagup \\ \circ \quad \circ \end{array} = \rho^4 \int d\mathbf{R} F(R) [[h(h * h)] * (h * h)](R) \quad (44)$$

$$\mathcal{E}_5^{(2)} = \frac{1}{2} \begin{array}{c} \bullet \\ \diagup \quad \diagdown \\ \bullet \quad \bullet \\ \diagdown \quad \diagup \\ \circ \cdots \circ \\ \bullet \\ \diagup \quad \diagdown \\ \bullet \quad \bullet \\ \diagdown \quad \diagup \\ \circ \quad \circ \end{array} = \frac{\rho^4}{2} \int d\mathbf{R} F(R) [h(h * h) * (h * h)](R) \quad (45)$$

$$\mathcal{E}_5^{(3)} = \begin{array}{c} \bullet \\ \diagup \quad \diagdown \\ \bullet \quad \bullet \\ \diagdown \quad \diagup \\ \circ \cdots \circ \\ \bullet \\ \diagup \quad \diagdown \\ \bullet \quad \bullet \\ \diagdown \quad \diagup \\ \circ \quad \circ \end{array} = \rho^4 \int d\mathbf{R} F(R) [h(h * h) * (h * h)](R) \quad (46)$$

$$\mathcal{E}_5^{(4)} = \begin{array}{c} \bullet \\ \diagup \quad \diagdown \\ \bullet \quad \bullet \\ \diagdown \quad \diagup \\ \circ \cdots \circ \\ \bullet \\ \diagup \quad \diagdown \\ \bullet \quad \bullet \\ \diagdown \quad \diagup \\ \circ \quad \circ \end{array} = \rho^4 \int d\mathbf{R} h(R) [h(F * h) * h(h * h)](R) \quad (47)$$

$$\mathcal{E}_5^{(5)} = \begin{array}{c} \bullet \\ \diagup \quad \diagdown \\ \bullet \quad \bullet \\ \diagdown \quad \diagup \\ \circ \cdots \circ \\ \bullet \\ \diagup \quad \diagdown \\ \bullet \quad \bullet \\ \diagdown \quad \diagup \\ \circ \quad \circ \end{array} = \rho^4 \int d\mathbf{R} F(R) [h(h * h) * h(h * h)](R) \quad (48)$$

$$\mathcal{E}_5^{(6)} = \frac{1}{2} \begin{array}{c} \bullet \\ \diagup \quad \diagdown \\ \bullet \quad \bullet \\ \diagdown \quad \diagup \\ \circ \cdots \circ \\ \bullet \\ \diagup \quad \diagdown \\ \bullet \quad \bullet \\ \diagdown \quad \diagup \\ \circ \quad \circ \end{array} = \frac{\rho^4}{2} \int d\mathbf{R} F(R) [h(h * h) * h(h * h)](R) \quad (49)$$

Above we have used standard notations: the continuous bond denote  $h = f^2 - 1$ , the dashed bond is  $F = v^* f^2$ , where  $f$  is the two body correlation function and  $v^* = v - \frac{\hbar^2}{2m_\alpha} \nabla^2 \ln f$  is the effective potential.

### 3.10 Concluding remarks

We devoted the research activity in 2012 to prepare software instruments in order to attack next year the main subject of this project: the ground state of neutral  $\alpha$ -matter using modern  $\alpha - \alpha$  potentials. In mean time we have published in 2 years a number of papers in international journals, most of them related with exotic matter in nuclear astrophysics (fusion at stellar energies, resonant diffraction, proton radiative capture, X-ray bursts).

### References

- [1] M. T. Johnson and J. W. Clark, *Variational Theory of Ideal Alpha Matter*, Kinam, **2**, 3 (1979).
- [2] G. P. Mueller and J.W. Clark , Nucl. Phys.**A155**, 561 (1970).
- [3] P. Darriulat, G. Igo, H. G. Pugh and H. D. Holmgren, Phys. Rev.**137**, B315 (1965).
- [4] S. Ali and A. R. Bodmer, Nucl. Phys.**A80** , 99 (1966).
- [5] T. Yamada and P. Schuck, Phys. Rev.**C69**, 024309 (2004).
- [6] W. S. Chien and R. E. Brown, Phys. Rev.**C10**, 1767 (1974).
- [7] F. Michel and G. Reidemeister, J. Phys.**G11**, 835(1985).
- [8] B. Buck, H. Friedrich and C. Wheatley, Nucl. Phys.**A275**, 246(1977)
- [9] V. G. Neudatchin, V. I. Kukulín, V. L. Korotkikh and V. P. Korennoy, Phys. Lett.**B34**, 581 (1971)
- [10] V. I. Kukulín, V. G. Neudatchin and Yu. F. Smirnov, Nucl. Phys.**A245**, 429 (1975)
- [11] L. Marquez, Phys. Rev.**C28**, 2525 (1983).
- [12] H. Takemoto et al., Phys. Rev.**C69**, 035802 (2004).
- [13] K. A. Gridnev et al., Int.J.Mod.Phys.E **14**, 635 (2005).
- [14] E. Feenberg, Ann. Phys.(N.Y.)**84**, 128 (1974).
- [15] F. Carstoiu and R.J. Lombard , Ann. Phys.(N.Y.)**217**, 279 (1992)
- [16] D. Gogny, in Proc. Int. Conf. on Nuclear Physics, eds. J. De Boer and H. Mang (North-Holland, Amsterdam, 1973)
- [17] J. Dechargé and D. Gogny, Phys. Rev.**C21**, 1568 (1980).

- [18] F. Chappert, M. Girod and S. Hilaire, Phys. Lett.**B668**, 420 (2008).
- [19] D. S. Delion, A. Sandulescu, Ş.Mişicu and F.Carstoiu and W.Greiner, Phys. Rev.**C64** 041303 (2001).
- [20] Ş. Mişicu and H. Esbensen, Phys. Rev. Lett.**91**, no.11, 112701 (2006).
- [21] J. S. Al-Khalili, J. A. Tostevin and I. J. Thompson, Phys. Rev.**C54**, 1843 (1996).
- [22] Ş. Mişicu and F. Carstoiu, Phys. Lett.**B682**, 33 (2009).
- [23] J. Benn, E. B. Dally, H. H. Müller, R. E. Pixley, H. H. Staub and H. Winkler, Phys.Lett.**20**, 43 (1966).
- [24] F. Carstoiu and M. Lassaut, Nucl. Phys.**A597**, 269 (1996).
- [25] R. E. Peierls and N. Vinh Mau, Nucl. Phys.**A343**, 1 (1980).
- [26] D. Baye, Phys. Rev. Lett. **58** 2738
- [27] D. Baye, J. Phys A:Math Gen **20** (1987) 5529 )
- [28] Newton R. G., *Scattering Theory of Waves and Particles*, (Springer, Berlin, 1982) 2nd ed.
- [29] K. Chadan and P.C. Sabatier, *Inverse Problems in Quantum Scattering Theory*
- [30] M. Lassaut, S. Y. Larsen, S. A. Sofianos and S. A. Rakityansky, J. Phys. A **34** 2007 (2001).
- [31] K. Chadan and A. Montes Lozano, Phys. Rev. **164**, 1762 (1967).
- [32] J. F. Berger, M. Girod, D. Gogny, Nucl. Phys.**A502**, 85c (1989).

## 4 Scientific activity 2013

### 4.1 Low energy $\alpha$ - $\alpha$ potentials

The phenomenological  $\alpha - \alpha$  potential of Ali and Bodmer [2] reproduces the low energy S-state phase shift but fails to reproduce the resonance properties in  $^8\text{Be}$ . The experimental properties of this resonance are  $E_{\text{res}} = 92.12 \pm 0.05$  keV,  $\Gamma_0 = 6.8 \pm 1.7$  eV [1]. This resonance could be correctly reproduced only by a renormalization of the repulsive component of the potential We have obtained four different parametrization which satisfy this constraint. These are dubbed AB0, AB1, AB2 and AB3 and have increasingly strong repulsive component.

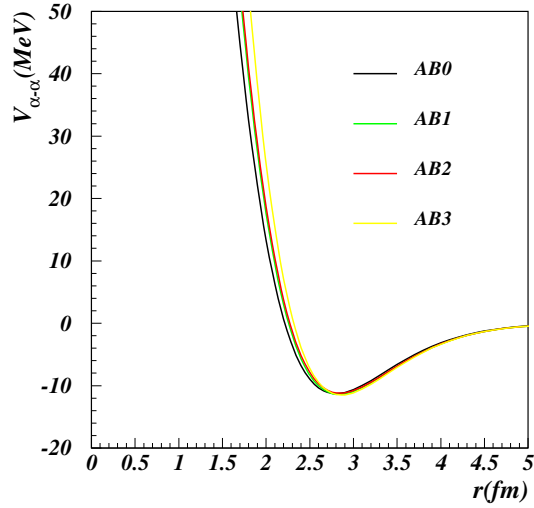


Figure 9: Renormalized Ali-Bodmer potentials which reproduce the phase shift and the properties of the S-state resonance in  $^8\text{Be}$

The low energy phase shift are compared in Fig.10 with the experimental data

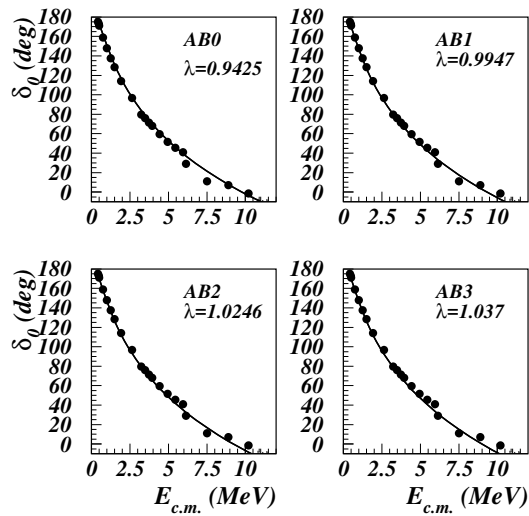


Figure 10: elastic scattering phase shift with renormalized AB potentials. The renormalization constant is  $\lambda$

The S-state resonance in  ${}^8\text{Be}$  is plotted in Fig.11

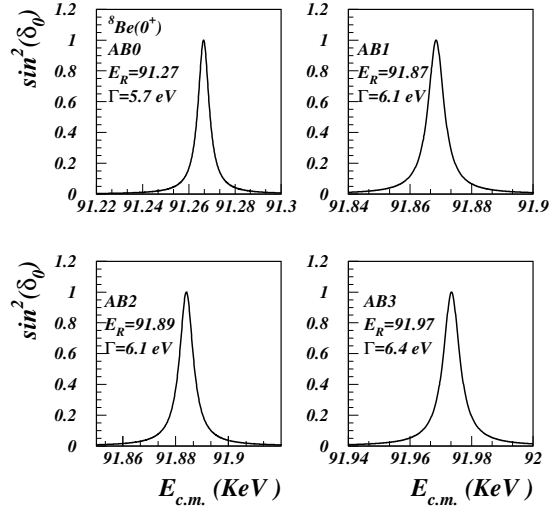


Figure 11: S-state resonance calculated with renormalized Ali-Bodmer potentials.

## 4.2 Ground state equation of $\alpha$ -matter at zero temperature.

The cluster expansion method was illustrated in the scientific report 2012 including all terms up to 4<sup>th</sup> order. a better assessment of convergence property of the cluster expansion could be established only if we go to next order. In the Percus-Yevick approximation the cluster expansion of the radial distribution function is illustrated in the next figure.

$$g(\mathbf{r}_{12}) = \begin{array}{c} \text{---} \\ \circ \\ \text{---} \\ \circ \end{array} + \begin{array}{c} \circ \\ \text{---} \\ \circ \end{array} + \begin{array}{c} \circ \quad \bullet \\ \text{---} \quad \text{---} \\ \circ \quad \bullet \end{array} + 2 \begin{array}{c} \circ \quad \bullet \\ \text{---} \quad \text{---} \\ \circ \quad \bullet \end{array} + \frac{1}{2} \begin{array}{c} \circ \quad \bullet \\ \text{---} \quad \text{---} \\ \circ \quad \bullet \end{array} + \frac{1}{2} \begin{array}{c} \circ \quad \bullet \\ \text{---} \quad \text{---} \\ \circ \quad \bullet \end{array} \\ + \begin{array}{c} \bullet \\ \text{---} \\ \bullet \end{array} + 2 \begin{array}{c} \bullet \\ \text{---} \\ \bullet \end{array} + \begin{array}{c} \bullet \\ \text{---} \\ \bullet \end{array} + 2 \begin{array}{c} \bullet \\ \text{---} \\ \bullet \end{array} \\ + 2 \begin{array}{c} \bullet \\ \text{---} \\ \bullet \end{array} + 2 \begin{array}{c} \bullet \\ \text{---} \\ \bullet \end{array} + \begin{array}{c} \bullet \\ \text{---} \\ \bullet \end{array}$$

In fact in the exact expansion there exist 24 5<sup>th</sup> order diagrams but only 7 main diagrams are considered in the PY approximation. The energy calculation corresponding to each diagram

implies a 15 order integral. Using folding numerical techniques, developed by the present author, we were able to obtain calculable expressions in a reasonable computing time,

$$E_{50} = \frac{1}{2}\rho^4 \int d\vec{R} F(R) \{ \eta * [\eta * (\eta * \eta)] \} (R) \quad (50)$$

$$E_{51} = \rho^4 \int d\vec{R}_1 F(R_1) \{ [\eta(\eta * \eta)] * (\eta * \eta) \} (R_1) \quad (51)$$

$$E_{52} = \frac{1}{2}\rho^4 \int d\vec{R}_1 F(R_1) \{ [\eta \cdot (\eta * \eta)] * [\eta * \eta] \} (R_1) \quad (52)$$

$$E_{53} = \rho^4 \int d\vec{R} F(R) \{ [\eta \cdot (\eta * \eta)] * (\eta * \eta) \} (R) \quad (53)$$

$$E_{54} = \rho^4 \int d\vec{R}_3 \eta(R_3) \{ \eta \cdot [F * \eta] \} * \{ \eta \cdot [\eta * \eta] \} \quad (54)$$

$$E_{56} = \frac{1}{2}\rho^4 \int d\vec{R}_1 F(R_1) ((\eta \cdot (\eta * \eta)) * (\eta \cdot (\eta * \eta))) (R_1)$$

in these equations  $f(r)$  is the two-particle correlation function,  $\eta = f^2 - 1$ ,  $F(r) = V^* f^2$ ,  $V^*$  is the Feinberg effective potential. For the first time we have obtained compact formulae for high order diagrams.

The cold  $\alpha$ -matter energy is illustrated in Fig.12.

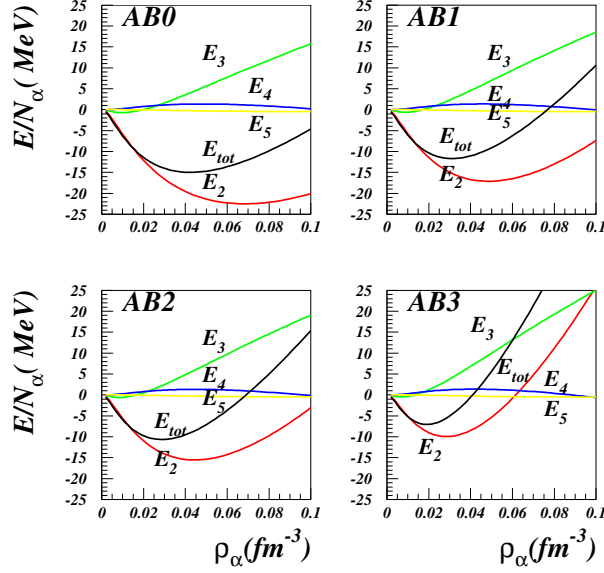
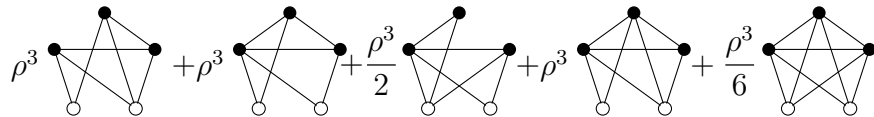


Figure 12: The total energy of  $\alpha$  matter is decomposed order by order

This figure illustrates our main result. Using density dependent correlation functions, the saturation effect appears even in the second order of the cluster expansion. The 3<sup>rd</sup> order diagram contributes repulsively to the total energy. The 4<sup>th</sup> and 5<sup>th</sup> order contribution are small and due to an evident cancellation effect ensure the convergence property of the cluster expansion series. Our essential result is that the equilibrium density depends mainly on the repulsive component of the interaction potential which prohibits strong overlaps of  $\alpha$ -particles. Thus, for the AB2 and AB3 parametrizations, the equilibrium density is about 0.2 particle/fm<sup>3</sup>, significantly less than the critical Mott value. The value of the equilibrium density corresponds to  $\rho = 0.08 \text{ fm}^{-3}$  in normal nuclear matter which corresponds to the nuclear surface in heavy nuclei. For the first time the  $\alpha$  clusterization in the nuclear surface is justified theoretically. Also the energy corresponding to the equilibrium density is close to the known energy of  $E = -16 \text{ MeV/A}$  if we take into account the internal energy of  $\alpha$  particle.

### 4.3 High order diagrams in the HNC approximation

To establish convincingly the convergence properties of the cluster expansion it is necessary to examine 5<sup>th</sup> order elementary diagrams contributing to the  $\alpha$ -matter energy in the HNC/5 approximation. The corresponding diagrams are depicted in the next figure



The numerical calculation of the corresponding energy is exceedingly time consuming, us-

ing the lowest order of the radial distribution function, i.e.  $g(r) = f^2(r)$ , with  $F(r)$  the density dependent correlation function previously defined, we succeeded to calculate the energy, see Fig.13. This result provides also a classification of the importance of the elementary diagrams. We concluded that in the HNC/5 approximation a single diagram saturates to total contribution of all 5<sup>th</sup> order diagram.

#### 4.4 Supersymmetric partners of the bare interactions

We have calculated the  $\alpha - \alpha$  potential in the double folding model including the knockon exchange term for the effective interaction Gogny D1. The nonlocal kernels were localized in the lowest order of the Perey-Saxon approximation. The wave functions for the redundant states 0s and 1s were calculated and eliminated by a supersymmetric transformation described above. The result is illustrated in Fig.14.

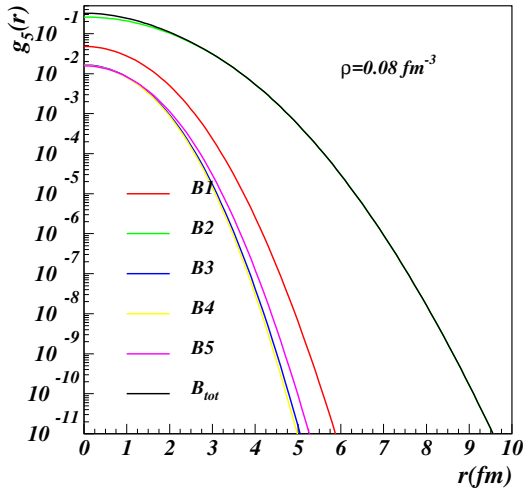


Figure 13: The radial distribution functions corresponding to the five order diagrams in the HNC approximation, calculated at a density  $\rho_\alpha = 0.08$ .

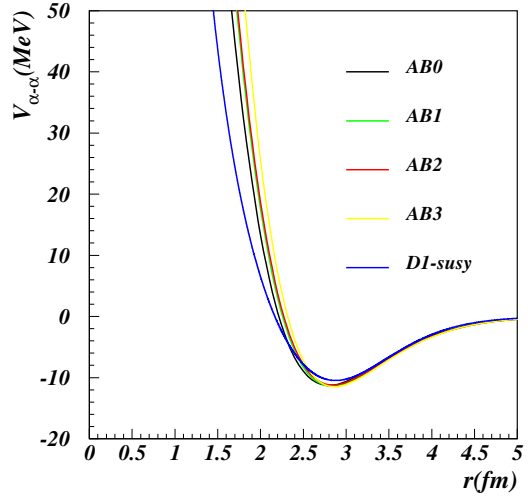


Figure 14: Supersymmetric partners corresponding to BFW and folding GOGNY are compared with potentials derived from Ali-Bodmer. All these potentials reproduce the experimental phase shift and the S-state resonance in  $^8\text{Be}$ .

## References

- [1] J. Benn, E. B. Dally, H. H. Müller, R. E. Pixley, H. H. Staub and H. Winkler, Phys.Lett.**20**, 43 (1966).
- [2] S. Ali and A. R. Bodmer, Nucl. Phys.**A80** , 99 (1966).

## 5 Scientific activity 2014

### 5.1 Introduction

During the year 2014 we concentrated our scientific activity on the study of convergence properties of cluster expansion method for calculating the ground state of the neutral alpha matter at zero temperature. The Cluster expansion method has a long history but the convergence properties of the series expansion have never been firmly established in the case of strongly interacting bosons. For example, in the case of alpha matter there are four diagrams of 4<sup>th</sup> order and 36 diagrams of 5<sup>th</sup> order to be calculated. Evidently this task is impossible within a reasonable computer time. We have to resort to a reasonable and well justified approximation. In the Percus-Yevick approximation the number of the 5<sup>th</sup> order diagrams are reduced to 7. We calculated these diagrams using folding techniques which allowed a rapid and precise evaluation of the contributions to the ground state energy. We found these contributions to be smaller by an order of magnitude compared to 4<sup>th</sup> order contributions in the entire range of alpha matter densities. The basic ingredient in these calculation is the alpha-alpha interaction potential at low energies. We started with the well known Ali-Bodmer potential and obtained several versions by constraining the potential to reproduce with high precision the scattering phase-shifts and the main properties of the first <sup>8</sup>Be J<sup>π</sup>=0<sup>+</sup> located at 0.92 KeV above the threshold. These two constrains are not sufficient to lead to an unique potential, but define quite well the class of potentials which lead to saturation. We further established the relation of these potentials with supersymmetric partners of the folding potentials generated by the Gogny D1 NN interaction. The single particle alpha density were taken from Bohigas and Stringari [1]slightly modified to reproduce the experimentally known charge formfactors at large momentum transfer. We found that saturation properties of the ground state energy depends essentially on the slope of the repulsive component in the alpha-alpha interaction. The lack of uniqueness of the potential is embarrassing, but fortunately this allows to give a palette of state equations as a function of alpha matter density. In all cases we found the saturation point near or below the critical point (Mott density). Our predicted EOS are quite shallow with a compressibility coefficient in the range of 130-160 MeV.

## 5.2 Astrophysical reaction rate for $^{17}\text{F}(p,\gamma)^{18}\text{Ne}$ from the transfer reaction $^{13}\text{C}(^{17}\text{O}, ^{18}\text{O})^{12}\text{C}$

Nucleosynthesis of elements in ONe white dwarf (WD) novae produces several sources of  $\gamma$ -ray lines. Among them is the positron-electron annihilation in the nova envelope, which leads to emission of a line at 511 keV and a continuum below it. It is believed that  $^{13}\text{N}$  ( $t_{1/2} = 9.965$  min) and  $^{18}\text{F}$  ( $t_{1/2} = 109.77$  min) are the main contributors to the production of observable positron annihilation radiation. Because of the short lifetime of  $^{13}\text{N}$ , the decay of  $^{18}\text{F}$  is more important since its  $\gamma$ -ray photons are emitted when the envelope starts to be transparent. According to the ONe models, when the temperature in the burning shell reaches  $T_9 \sim 0.2$ - $0.4$ , the main nuclear activity to produce  $^{18}\text{F}$  is driven by a  $\beta$ -decay following the proton capture reaction  $^{17}\text{F}(p,\gamma)^{18}\text{Ne}$ . This is an important reaction that is interesting to be studied to understand the unobserved 511 keV lines after the explosion. The rate of this reaction may influence the abundances of  $^{18}\text{F}$ ,  $^{18}\text{Ne}$ ,  $^{17}\text{F}$ , and  $^{15}\text{O}$ , and explain the transition sequence from the HCNO cycle to the rp-process. The nuclear structure of  $^{18}\text{Ne}$  depends on the configurations and the binding energy of the levels in the mirror nucleus  $^{18}\text{O}$  taking into account the Coulomb energies. Shell model calculations assume a  $2s$  or  $1d$  nucleon coupled to the single particle  $5/2+$ ,  $1/2+$ , and  $3/2+$  levels of  $^{17}\text{O}$  and  $^{17}\text{F}$ . Comparison of the nuclear structure of the mirror nuclei for the low-lying states shows that their excitation energies are very similar as reported in [2]. The rate of  $^{17}\text{F}(p,\gamma)^{18}\text{Ne}$  reaction has been determined by applying several theoretical methods and experimental measurements. Wiescher, Gorres, and Thielmann noticed that the  $J^\pi = 3+$  level in  $^{18}\text{Ne}$  greatly influences the thermonuclear reaction rate [3]. Recent experiments have obtained precise information about the energy of the  $3+$  level,  $E_x = 4.525(0.002)$  MeV, and its total width,  $\Gamma_p = 18(2)$  keV [4, 5]. Estimates of the reaction rate show that the resonant capture to the  $3+$  state dominates the rate only at  $T_9 \sim 0.5$  [4], which is an appropriate temperature for explosive events such as x-rays bursts and supernovas. The direct reaction measurement for  $^{17}\text{F}(p,\gamma)^{18}\text{Ne}$  at ORNL shows that astrophysical importance of the resonant contribution is increased by a factor of 10 in those events [6]. A slight complication occurs from the fact that  $^{18}\text{Ne}$  is an even- $Z$  nucleus, and its states can have more than one proton orbital involved. There are four proton bound states in  $^{18}\text{Ne}$  and direct radiative proton capture can proceed via any and all of them. The nuclear cross section predicts that the  $^{17}\text{F}(p,\gamma)^{18}\text{Ne}$  reaction will be dominated by direct capture to the lowest energy  $J^\pi = 2+$  states, mainly at  $E_x = 1.887$  MeV and  $E_x = 3.616$  MeV.

The experiment was carried out with two separate 12 MeV/u  $^{17}\text{O}$  and  $^{18}\text{O}$  beams from K500 superconducting cyclotron at Texas A&M University. Each beam was transported through the beam analysis system to the scattering chamber of the multipole-dipole- multipole (MDM) magnetic spectrometer [9], where it interacted with  $100 \mu\text{g}/\text{cm}^2$  target. We have measured the neutron pick-up from the loosely bound nucleus  $^{13}\text{C}$  and two elastic scattering cross sections for the incoming and outgoing channels. First, the  $^{17}\text{O}$  beam was impinged on  $^{13}\text{C}$  target. The elastic scattering angular distribution was measured for the spectrometer angles  $4^\circ$ - $25^\circ$  in the laboratory system. The  $4^\circ \times 1^\circ$  wide-opening mask and an angle mask consisting of

five narrow  $\Delta\theta=0.1^\circ$  slits were used for each spectrometer angle to double-check the absolute values of the cross section and the quality of the angle calibration. Fine tuned RAYTRACE [10] calculations were used to reconstruct the position of particles in the focal plane and the scattering angle at the target. The instrumental setup, including the focal plane detector, and processes for energy and angle calibrations, are identical to that described in Ref. [11]. Second, the  $^{12}\text{C}$  target was bombarded by  $^{18}\text{O}$  beam with 216 MeV total laboratory energy. The elastic scattering cross section was measured at  $4^\circ$ - $22^\circ$  spectrometer angles. The quality of the angular resolution,  $\Delta\theta_{res}$ , of the detector in both cases was on average  $0.31^\circ$  in c.m. frame and the position resolution was better than 1 mm.

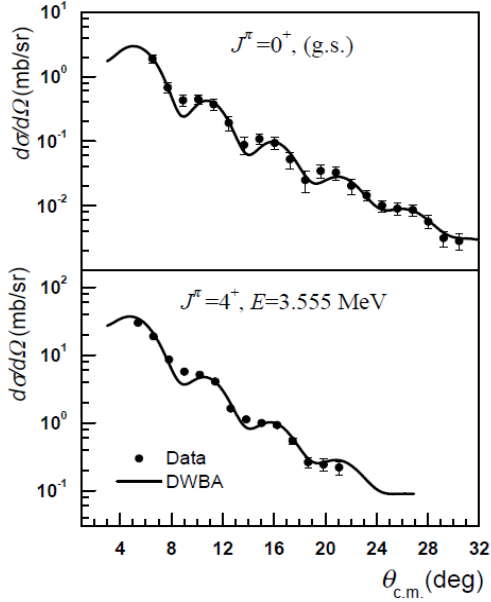


Figure 15: The angular distribution for populating (a) the ground state and (b) the  $4+$  state in  $^{18}\text{O}$ . The points are the experimental data and the solid curve the DWBA cross section.

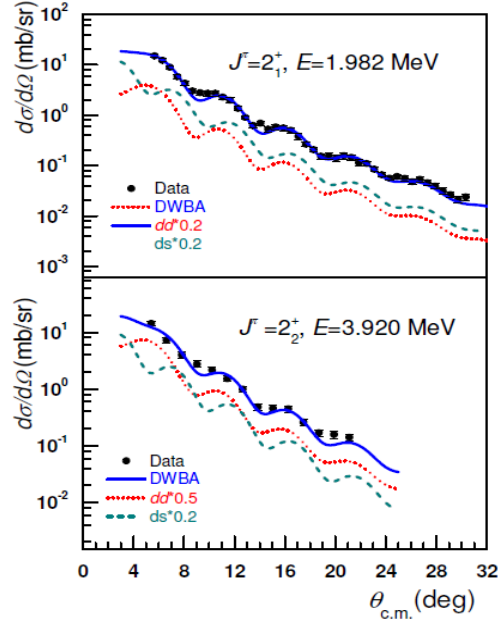


Figure 16: The angular distribution for populating (a) the  $2_1^+$  state and (b) the  $2_2^+$  state in  $^{18}\text{O}$ . The points are the experimental data and the solid curve the DWBA cross section obtained as incoherent sum of the  $dd$  and  $ds$  configurations.

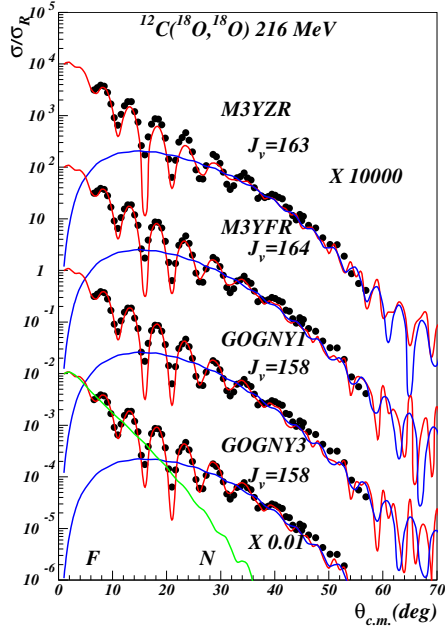


Figure 17: Angular distribution calculated with selected effective NN interactions.

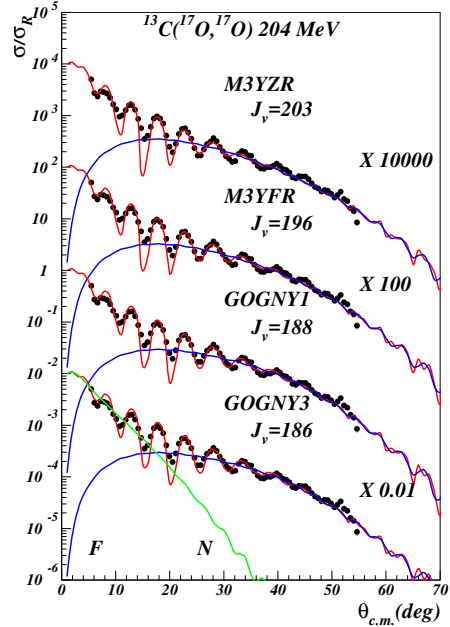


Figure 18: The same as in Fig. 25 but for the other reaction.

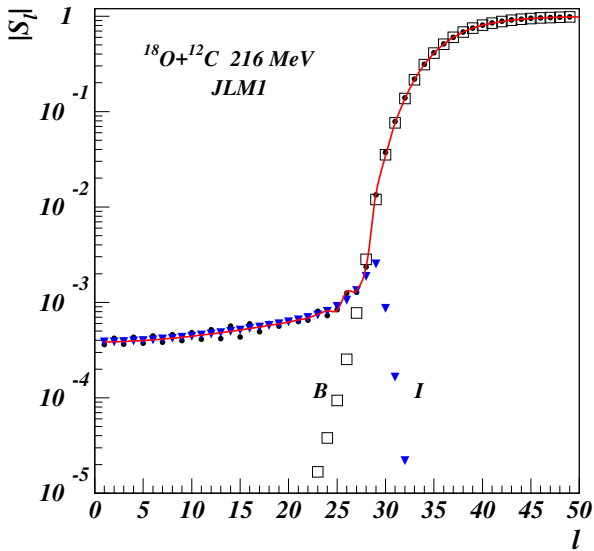


Figure 19: Absorption profile for the S-matrix calculated with JLM1 effective interaction. The semiclassical S-matrix is decomposed into barrier (B) and internal barrier (I) components. The internal barrier component is small demonstrating that the reaction is peripheral.

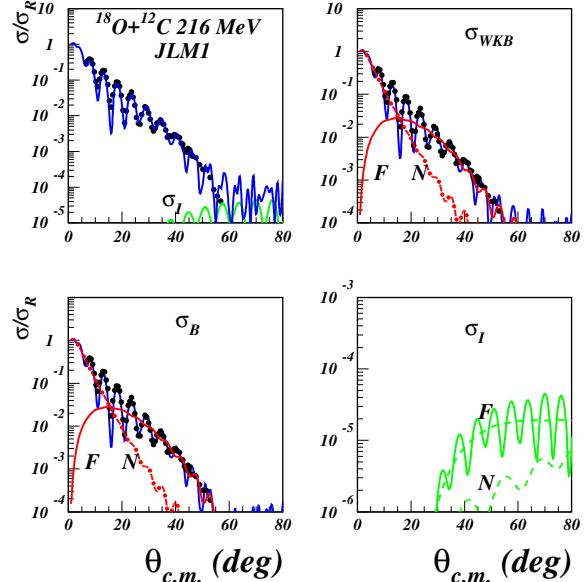


Figure 20: Semiclassical calculation of the elastic scattering. The barrier and internal barrier components are shown in separate panels. The internal barrier cross section is small each component is further decomposed into far side/near side subcomponents.

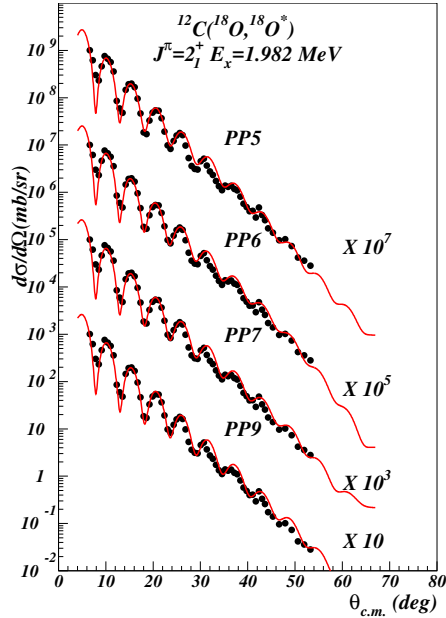


Figure 21: Inelastic cross sections calculated with phase equivalent WS potentials.

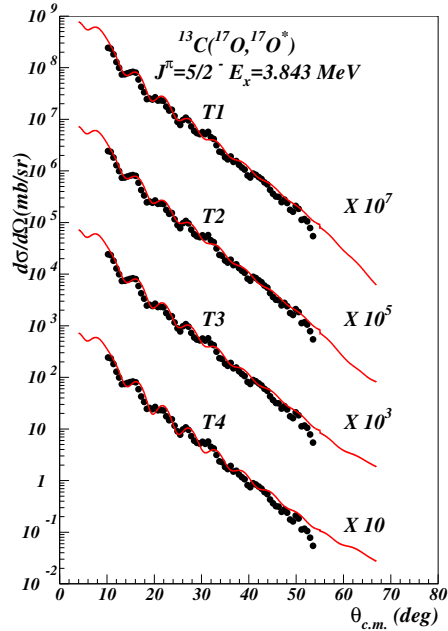


Figure 22: Inelastic cross sections calculated with phase equivalent WS potentials.

### 5.3 References

- 1 A. Coc, M. Hrenanz, J. Jose, and J. Thibaud, *Astron. Astrophys.* 357, 561 (2000).
- 2 R. Sherr and H. F. Fortune, *Phys. Rev. C* 58, 3292 (1998).
- 3 M. Wiescher, J. Gorres, and F.-K. Thielemann, *Astrophys. J.* 326, 384 (1988).
- 4 D. W. Bardayan, J. C. Blackmon<sup>1</sup>, C. R. Brune, A. E. Champagne<sup>3</sup>, A. A. Chen<sup>2</sup>, J. M. Cox<sup>4</sup>, T. Davinson<sup>5</sup>, V. Y. Hansper, M. A. Hofstee, B. A. Johnson, et al., *Comp. Phys. Comm.* 62, 055804 (2000).
- 5 Y. Parpottas, S. M. Grims, S. Al-Quraishi, C. R. Brune, T. N. Massey, J. E. O'Donnell, J. E. Oldendick, A. Salas, and R. T. Wheeler, *Phys. Rev. C* 72, 025802 (2005).
- 6 K. A. Chipps, D. W. Bardayan, J. C. Blackmon, K. Y. Chae, U. Greife, R. Hatarik, R. L. Kozub, C. Matei, B. H. Moazen, C. D. Nesaraja, et al., *Phys. Rev. Lett.* 102, 152502

(2009)

- 7 A. Garcia, E. G. Adelberger, P. V. Magnus, D. M. Marko, K. B. S. M. S. Smith, K. I. Hahn, N. Bateman, and P. D. Parker, *Phys. Rev. C* 43, 2012 (2003).
- 8 T. K. Li, D. Dehnhard, R. E. Brown, and P. J. Ellis, *Phys. Rev. C* 13, 55 (1976).
- 9 D. M. Pringle, W. N. Catford, J. S. Wineld, D. G. Lewis, N. A. Jelley, K. W. Allen, and J. H. Coupland, *Nucl. Instrum. Methods Phys. Res. A* 245, 230 (1986).
- 10 S. Kowalski and H. A. Enge, computer code RAYTRACE (unpublished), University of Oxford, England, UK, 1986.
- 11 A. M. Mukhamedzhanov, V. Burjan, F. Carstoiu, J. Cejpek, H. L. Clark, C. A. Gagliardi, Y.-W. Lui, V. Kroha, L. Trache, R. E. Tribble, et al., *Phys. Rev. C* 56, 1302 (1997).

## 6 Scientific activity 2015

### 6.1 Introduction

We have a long-term program to understand and describe nucleus-nucleus collisions in terms of one body interaction potential, the optical model potential (OMP). A good understanding of all phenomena occurring in the elastic nucleus-nucleus scattering, which are used typically to extract OMP, and the interpretation of the origin of different aspects, including the well known potential ambiguities, are of crucial importance for finding and justifying the procedures used for predicting nucleus-nucleus OMP in the era of radioactive nuclear beams (RNB), including ours based on double folding [1]. The reliability of these potentials is crucial for the correct description of a number of reactions involving RNBs, from elastic to transfer and breakup, at energies ranging from a few to a few hundred MeV/nucleon. Of particular interest for us is to support the absolute values of the calculated cross sections for reactions used in indirect methods for nuclear astrophysics, see [2] and [3] for the most recent results. In this framework, we treat here the case of heavy ion orbiting, one of the phenomena found over the years to occur in special cases of elastic scattering, well understood semi-classically, but not well documented by specific examples.

## References

- [1] L. Trache, A. Azhari, H. L. Clark, C. A. Gagliardi, Y.-W. Lui, A. M. Mukhamedzhanov, X. Tang, N. Timofeyuk, R. E. Tribble and F. Carstoiu, Phys. Rev. **C61**, 024612 (2000).
- [2] T. Al-Abdullah, F. Carstoiu, X. Chen, H. L. Clarke, C. A. Gagliardi, Y.-W. Lui, A. Mukhamedzhanov, G. Tabacaru, Y. Takimoto, L. Trache, R.E.Tribble, Y. Zhai Phys. Rev. C **89**, 025809 ( 2014).
- [3] T. Al-Abdullah, F. Carstoiu, C. A. Gagliardi, G. Tabacaru, L. Trache and R. E. Tribble. Phys. Rev. C **89**, 064602 (2014).

## 6.2 Nuclear reactions in the explosive stage of supernovas

### 6.2.1 Astrophysical reaction rate for $^{17}\text{F}(p,\gamma)^{18}\text{Ne}$ from the transfer reaction $^{13}\text{C}(^{17}\text{O},^{18}\text{O})^{12}\text{C}$ . Peripheral reactions of $^{17,18}\text{O}$ on light targets.

Paper:

Peripheral elastic and inelastic scattering of  $^{17,18}\text{O}$  on light targets at 12 MeV/nucleon

F. Carstoiu, T. Al-Abdullah, C. A. Gagliardi and L. Trache

AIP Conference proceedings, vol 1645, p39 (2015)

Carpathian Summer Scool of Physics, Sinaia, 13-26 July, 2014

Nucleosynthesis of elements in ONe white dwarf (WD) novae produces several sources of  $\gamma$ -ray lines. Among them is the positron-electron annihilation in the nova envelope, which leads to emission of a line at 511 keV and a continuum below it. It is believed that  $^{13}\text{N}$  ( $t_{1/2} = 9.965$  min) and  $^{18}\text{F}$  ( $t_{1/2} = 109.77$  min) are the main contributors to the production of observable positron annihilation radiation. Because of the short lifetime of  $^{13}\text{N}$ , the decay of  $^{18}\text{F}$  is more important since its  $\gamma$ -ray photons are emitted when the envelope starts to be transparent. According to the ONe models, when the temperature in the burning shell reaches  $T_9 \sim 0.2-0.4$ , the main nuclear activity to produce  $^{18}\text{F}$  is driven by a  $\beta$ -decay following the proton capture reaction  $^{17}\text{F}(p,\gamma)^{18}\text{Ne}$ . . This is an important reaction that is interesting to be studied to understand the unobserved 511 keV lines after the explosion. The rate of this reaction may influence the abundances of  $^{18}\text{F}$ ,  $^{18}\text{Ne}$ ,  $^{17}\text{F}$ , and  $^{15}\text{O}$ , and explain the transition sequence from the HCNO cycle to the rp-process. The nuclear structure of  $^{18}\text{Ne}$  depends on the configurations and the binding energy of the levels in the mirror nucleus  $^{18}\text{O}$  taking into account the Coulomb energies. Shell model calculations assume a  $2s$  or  $1d$  nucleon coupled to the single particle  $5/2+$ ,  $1/2+$ , and  $3/2+$  levels of  $^{17}\text{O}$  and  $^{17}\text{F}$ . Comparison of the nuclear structure of the mirror nuclei for the low- lying states shows that their excitation energies are very similar as reported in [2]. The rate of  $^{17}\text{F}(p,\gamma)^{18}\text{Ne}$  reaction has been determined by applying several theoretical methods

and experimental measurements. Wiescher, Gorres, and Thielmann noticed that the  $J^\pi = 3+$  level in  $^{18}\text{Ne}$  greatly influences the thermonuclear reaction rate [3]. Recent experiments have obtained precise information about the energy of the  $3+$  level,  $E_x = 4.525(0.002)$  MeV, and its total width,  $\Gamma_p = 18(2)$  keV [4, 5]. Estimates of the reaction rate show that the resonant capture to the  $3+$  state dominates the rate only at  $T_9 \sim 0.5$  [4], which is an appropriate temperature for explosive events such as x-rays bursts and supernovas. The direct reaction measurement for  $^{17}\text{F}(p,\gamma)^{18}\text{Ne}$  at ORNL shows that astrophysical importance of the resonant contribution is increased by a factor of 10 in those events [6]. A slight complication occurs from the fact that  $^{18}\text{Ne}$  is an even- $Z$  nucleus, and its states can have more than one proton orbital involved. There are four proton bound states in  $^{18}\text{Ne}$  and direct radiative proton capture can proceed via any and all of them. The nuclear cross section predicts that the  $^{17}\text{F}(p; \gamma)^{18}\text{Ne}$  reaction will be dominated by direct capture to the lowest energy  $J^\pi = 2+$  states, mainly at  $E_x = 1.887$  MeV and  $E_x = 3.616$  MeV. The experiment was carried out with two separate 12 MeV/u  $^{17}\text{O}$

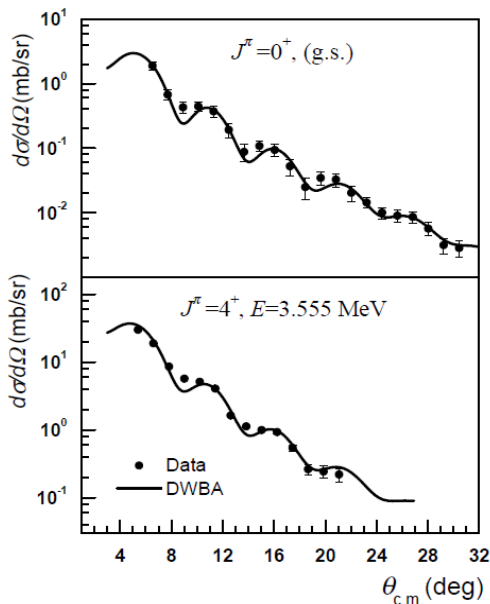


Figure 23: The angular distribution for populating (a) the ground state and (b) the  $4+$  state in  $^{18}\text{O}$ . The points are the experimental data and the solid curve the DWBA cross section.

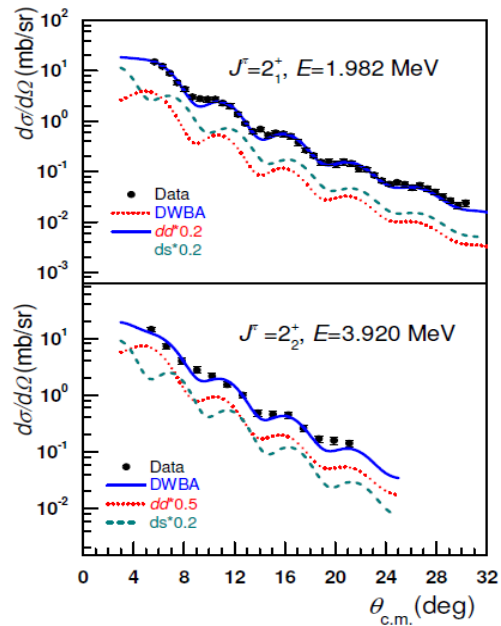


Figure 24: The angular distribution for populating (a) the  $2_1^+$  state and (b) the  $2_2^+$  state in  $^{18}\text{O}$ . The points are the experimental data and the solid curve the DWBA cross section obtained as incoherent sum of the  $dd$  and  $ds$  configurations.

and  $^{18}\text{O}$  beams from K500 superconducting cyclotron at Texas A&M University. Each beam was transported through the beam analysis system to the scattering chamber of the multipole-dipole- multipole (MDM) magnetic spectrometer [9], where it interacted with  $100 \mu\text{gm}/\text{cm}^2$  target. We have measured the neutron pick-up from the loosely bound nucleus  $^{13}\text{C}$  and two

elastic scattering cross sections for the incoming and outgoing channels. First, the  $^{17}\text{O}$  beam was impinged on  $^{13}\text{C}$  target. The elastic scattering angular distribution was measured for the spectrometer angles  $4^\circ$ - $25^\circ$  in the laboratory system. The  $4^\circ \times 1^\circ$  wide-opening mask and an angle mask consisting of five narrow  $\Delta\theta = 0.1^\circ$  slits were used for each spectrometer angle to double-check the absolute values of the cross section and the quality of the angle calibration. Fine tuned RAYTRACE [10] calculations were used to reconstruct the position of particles in the focal plane and the scattering angle at the target. The instrumental setup, including the focal plane detector, and processes for energy and angle calibrations, are identical to that described in Ref. [11]. Second, the  $^{12}\text{C}$  target was bombarded by  $^{18}\text{O}$  beam with 216 MeV total laboratory energy. The elastic scattering cross section was measured at  $4^\circ$ - $22^\circ$  spectrometer angles. The quality of the angular resolution,  $\Delta\theta_{res}$ , of the detector in both cases was on average  $0.31^\circ$  in c.m. frame and the position resolution was better than 1 mm.

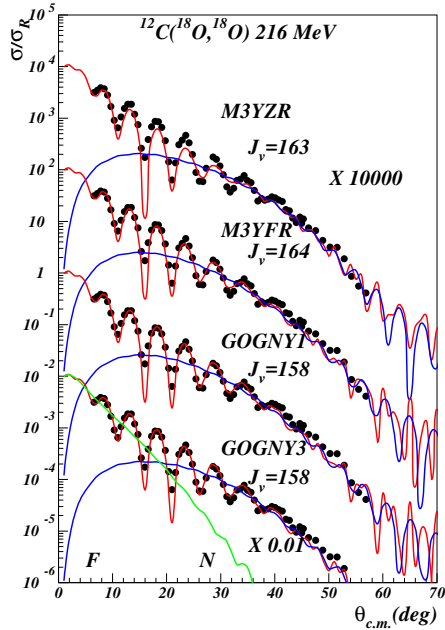


Figure 25: Angular distribution calculated with selected effective NN interactions.

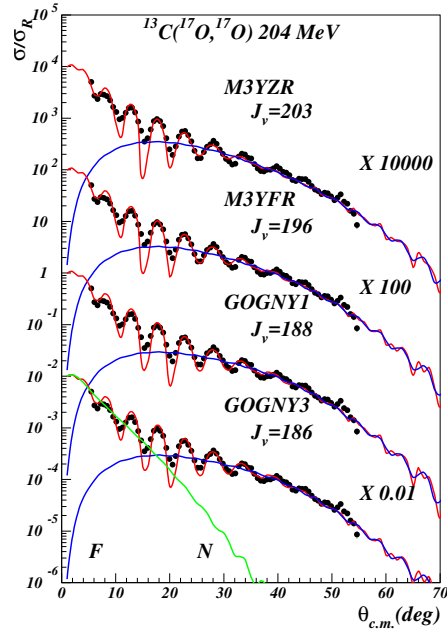


Figure 26: The same as in Fig. 25 but for the other reaction.

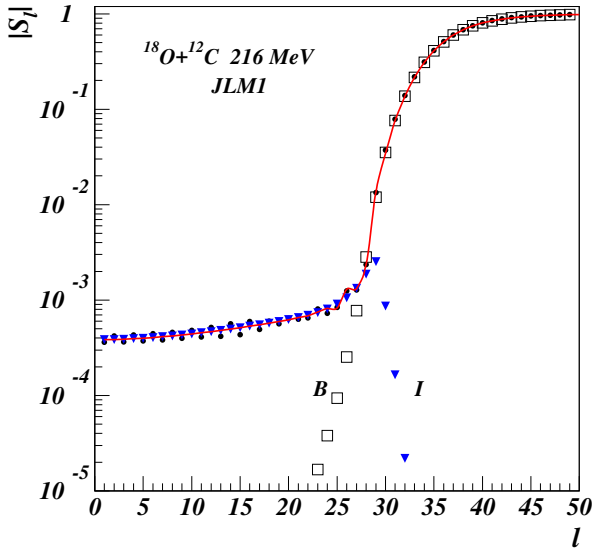


Figure 27: Absorption profile for the S-matrix calculated with JLM1 effective interaction. The semiclassical S-matrix is decomposed into barrier (B) and internal barrier (I) components. The internal barrier component is small demonstrating that the reaction is peripheral.

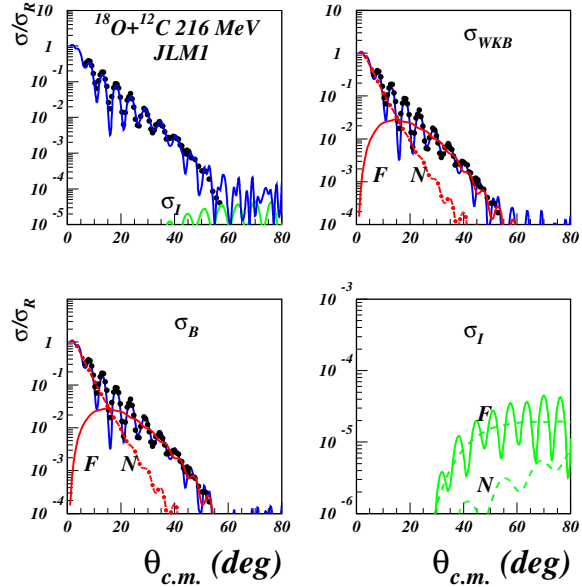


Figure 28: Semiclassical calculation of the elastic scattering. The barrier and internal barrier components are shown in separate panels. The internal barrier cross section is small each component is further decomposed into far side/near side subcomponents.

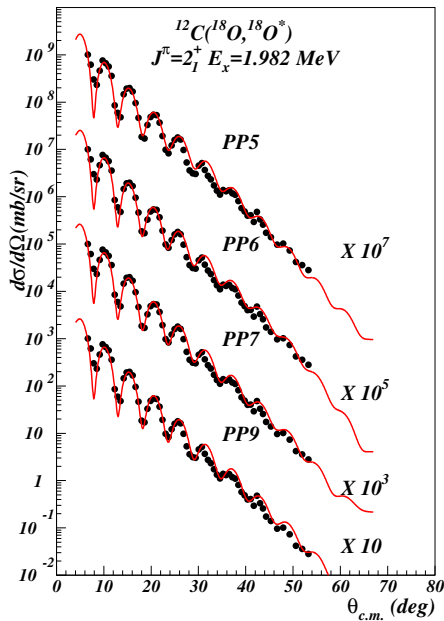


Figure 29: Inelastic cross sections calculated with phase equivalent WS potentials.

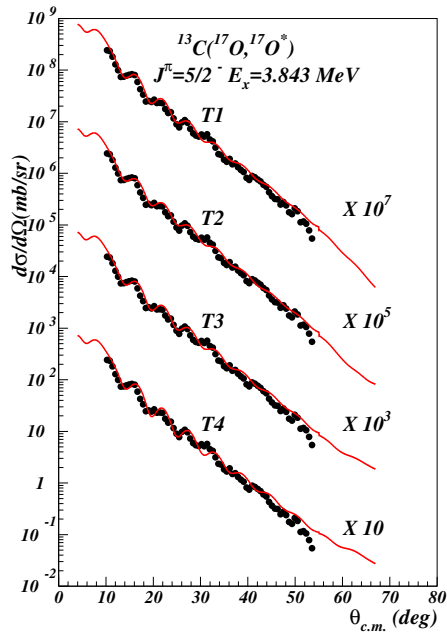


Figure 30: Inelastic cross sections calculated with phase equivalent WS potentials.

- 1 A. Coc, M. Hrenanz, J. Jose, and J. Thibaud, *Astron. Astrophys.* 357, 561 (2000).
- 2 R. Sherr and H. F. Fortune, *Phys. Rev. C* 58, 3292 (1998).
- 3 M. Wiescher, J. Gorres, and F.-K. Thielemann, *Astrophys. J.* 326, 384 (1988).
- 4 D. W. Bardayan, J. C. Blackmon<sup>1</sup>, C. R. Brune, A. E. Champagne<sup>3</sup>, A. A. Chen<sup>2</sup>, J. M. Cox<sup>4</sup>, T. Davinson<sup>5</sup>, V. Y. Hansper, M. A. Hofstee, B. A. Johnson, et al., *Comp. Phys. Comm.* 62, 055804 (2000).
- 5 Y. Parpottas, S. M. Grims, S. Al-Quraishi, C. R. Brune, T. N. Massey, J. E. O'Donnell, J. E. Oldendick, A. Salas, and R. T. Wheeler, *Phys. Rev. C* 72, 025802 (2005).
- 6 K. A. Chipps, D. W. Bardayan, J. C. Blackmon, K. Y. Chae, U. Greife, R. Hatarik, R. L. Kozub, C. Matei, B. H. Moazen, C. D. Nesaraja, et al., *Phys. Rev. Lett.* 102, 152502 (2009).
- 7 A. Garcia, E. G. Adelberger, P. V. Magnus, D. M. Marko, K. B. S. M. S. Smith, K. I. Hahn, N. Bateman, and P. D. Parker, *Phys. Rev. C* 43, 2012 (2003).
- 8 T. K. Li, D. Dehnhard, R. E. Brown, and P. J. Ellis, *Phys. Rev. C* 13, 55 (1976).
- 9 D. M. Pringle, W. N. Catford, J. S. Wineld, D. G. Lewis, N. A. Jelley, K. W. Allen, and J. H. Coupland, *Nucl. Instrum. Methods Phys. Res. A* 245, 230 (1986).
- 10 S. Kowalski and H. A. Enge, computer code RAYTRACE (unpublished), University of Oxford, England, UK, 1986.
- 11 A. M. Mukhamedzhanov, V. Burjan, F. Carstoiu, J. Cejpek, H. L. Clark, C. A. Gagliardi, Y.-W. Lui, V. Kroha, L. Trache, R. E. Tribble, et al., *Phys. Rev. C* 56, 1302 (1997).

### 6.3 Mathematical physics

Wei-Norman and Berezin's equations of motion on the Siegel-Jacobi disk

S. Berceanu

*Rom. J. Phys.*, Vol.60, fasc.1-2, p.126-146, 2015.

It is shown that the Wei-Norman method applied to describe the evolution on the Siegel-Jacobi disk  $\mathcal{D}_1^J = \mathcal{D}_1 \times \mathbb{C}^1$ , where  $\mathcal{D}_1$  denotes the Siegel disk, determined by a hermitian Hamiltonian linear in the generators of the Jacobi group  $G_1^J$  and Berezin's scheme using coherent states give the same equations of quantum and classical motion when are expressed in the coordinates in which the Kähler two-form  $\omega_{\mathcal{D}_1^J}$  can be written as  $\omega_{\mathcal{D}_1^J} = \omega_{\mathcal{D}_1} + \omega_{\mathbb{C}^1}$ . The Wei-Norman equations on  $\mathcal{D}_1^J$  are a particular case of equations of motion on the Siegel-Jacobi ball  $\mathcal{D}_n^J$  generated by a hermitian Hamiltonian linear in the generators of the Jacobi group  $G_n^J$

obtained in Berezin's approach based on coherent states on  $\mathcal{D}_n^J$ .

Bergman representative coordinates on the Siegel-Jacobi disk  
Rom. J. Phys., Vol.60, fasc.7-8, p. 867-896, 2015  
S. Berceanu

We underline some differences between the geometric aspect of Berezin's approach to quantization on homogeneous Kähler manifolds and Bergman's construction for bounded domains in  $\mathbb{C}^n$ . We construct explicitly the Bergman representative coordinates for the Siegel-Jacobi disk  $\mathcal{D}_1^J$ , which is a partially bounded manifold whose points belong to  $\mathbb{C} \times \mathcal{D}_1$ , where  $\mathcal{D}_1$  denotes the Siegel disk. The Bergman representative coordinates on  $\mathcal{D}_1^J$  are globally defined, the Siegel-Jacobi disk is a normal Kähler homogeneous Lu Qi-Keng manifold, whose representative manifold is the Siegel-Jacobi disk itself.

## 6.4 New experiment proposal

In 2014 we reported a proposal for an experiment in collaboration with LOUISIANA (dr. J. Blackmon), RIKEN ( prof. Motobayashi, dr. Yoneda), TEXAS A&M (prof. Tribble). IFIN-HH (dr. Carstoiu, dr. Trache), to be performed at SAMURAI, RIKEN, JAPAN. The proposal was initially scheduled for 2015, but the circumstances were changed.

### **Proposal title:**

Study of the  $^{27}\text{P}(p,\gamma)^{28}\text{S}$  and  $^{31}\text{Cl}(p,\gamma)^{32}\text{Ar}$  Reactions that are Important for X-ray Burst Light Curves

We report here a second proposal for which theoretical simulation were performed in Bucharest.

### **Title of Project**

Breakup of loosely bound nuclei at intermediate energies for nuclear astrophysics and the development of a position sensitive microstrip detector system and its readout electronics using ASICs technologies.

### **Applicant/Institution:**

Cyclotron Institute, Texas A&M University MS 3366 College Station, TX 77843-3366

### **Principal Investigator:** Prof. Robert E. Tribble

Texas A&M University

### **Participating institutions:**

Cyclotron Institute, Texas A&M University, College Station, TX R.E. Tribble, L. Trache, A. Banu, B. Roeder

Departments of Chemistry and Physics, Washington University, St. Louis, MO L.G. Sobotka, R.J. Charity, J.M. Elson, G.L. Engel (South Illinois Univ. Edwardsville)

Department of Physics, Louisiana State University, Baton Rouge, LA

J. C. Blackmon

Department of Physics, Texas A&M University, Commerce, TX C.A. Bertulani,  
Cyclotron Institute, MS 3366  
College Station, TX 77843-3366

**International collaborators:** F. Carstoiu ( IFIN-HH Bucharest, Romania),  
N. Orr (LPC Caen, Univ de Caen, France)  
A. Bonaccorso (INFN, Sezione di Pisa, Italy),  
D. Brink (Oxford Univ., UK)

### **Scientific goals**

We plan to carry out a physics program by performing a series of experiments with rare isotopes beams (RIBs) at RIBF. Initially, we will focus on proton-breakup (or one-proton removal) reactions at intermediate energies. We will use these data to better understand the single particle properties of proton-rich nuclei close to the drip line, to determine Asymptotic Normalization Constants (ANC) and, from them, reaction rates of importance in H-burning in explosive nucleosynthesis. We plan to extend this in the future to develop techniques that can be used to better understand neutron capture reaction rates as well, as RIBF will be a facility with beams and instrumentation aimed toward studying neutron-rich nuclei.

### **Breakup reactions for nuclear astrophysics studies**

Among the arguments to study rare isotopes, as expressed in the recent U.S. Long Range Plan, a very important one is to provide information that is needed to better understand explosive nuclear synthesis. To make reliable predictions for the synthesis of chemical elements and the evolution of stars and galaxies, we need several types of data, including the rates of nuclear reactions that provide the energy in nuclear synthesis, especially explosive processes. Stellar nucleosynthesis processes typically involve unstable nuclei. For most of those, we have currently only limited knowledge about their corresponding reaction rates. Direct measurements for nuclear astrophysics involving unstable nuclei are difficult for two reasons: a) targets (or projectiles at appropriate energies for inverse kinematics) of unstable nuclei are not easily available, if at all, and b) charged-particle reactions at the very low energies relevant for stellar processes are very difficult to measure due to the Coulomb repulsion, which leads to very low reaction cross sections. Hence, very few direct measurements have been done on unstable nuclei to date. This problem has led to the development and use of indirect methods in nuclear astrophysics. The list of indirect techniques that are used includes Coulomb dissociation, transfer reactions (the ANC method), breakup at intermediate energies, the Trojan horse method, and spectroscopic studies, in particular the location of resonance states and the determination of resonance parameters. It has been demonstrated that nuclear breakup experiments at intermediate energies can be used to obtain information of importance to nuclear astrophysics. From the nuclear breakup of radioactive nuclei with the emission of a proton, one can extract asymptotic normalization coefficients (ANCs) for the  $X \rightarrow Y + p$  system. This information is

sufficient to determine the non-resonant contribution to the reaction rate for radiative proton capture,  $Y(p,\gamma)X$ , at stellar temperatures, which is the major contribution at stellar energies in a large number of reactions important in nuclear astrophysics, in particular for explosive H-burning. The experimental method employed in these studies, which is shown schematically in Fig. 31, involves breakup in the nuclear field of the target (as opposed to the Coulomb field). It is a highly peripheral process for a large range of projectile energies. The energies depend on the particular nuclei, mostly on the binding energy and the orbital momentum of the single particle orbitals involved in the breakup, but are generally in the intermediate energy range (100 A-MeV) accessible to RIBF at RIKEN. Gamma-ray detectors are used in these experiments to understand the configuration mixing in the structure of projectiles.

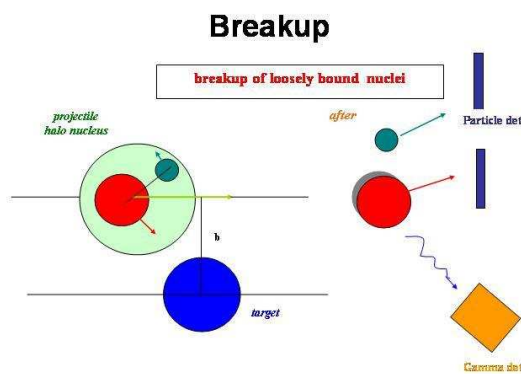


Figure 31: Schematic representation of breakup reaction

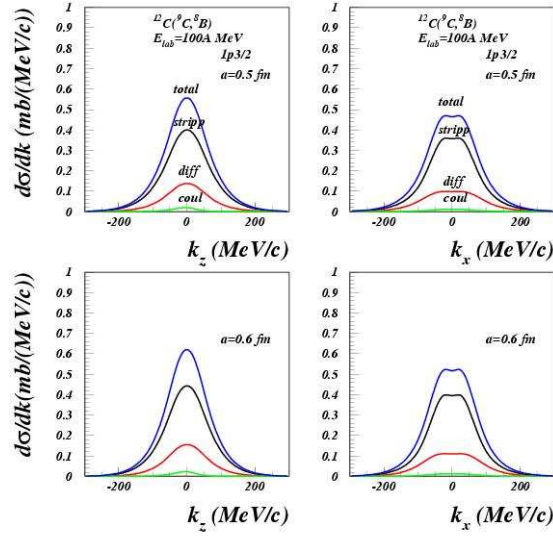


Figure 32: Theoretical estimation of the one proton breakup of  ${}^9\text{C}$  at 100 MeV/A. The parallel and perpendicular momentum distributions is calculated for single particle potential with diffusivity parameter  $a=0.6$  fm. The valence nucleon wave function is assumed to be a pure  $1p_{3/2}$  state. The total cross section includes stripping, diffraction and Coulomb breakup.

## 7 Scientific activity 2016

### 7.1 Heavy ion orbiting and Regge poles

Heavy ion orbiting is one of the phenomena found over the years to occur in special case of elastic scattering, well understood semi-classically, but not well documented by specific examples.

The anomalous large-angle scattering of  $\alpha$ -particles at moderate energies from elements throughout the periodic table has been a subject of considerable experimental study and has evoked a wide range of novel theoretical explanations [4, 5]. The conventional nuclear optical potential can explain much, if not all, of the anomalous scattering. The dominant physical parameter determining back-angle scattering is the strength,  $W$ , of the imaginary part of the optical potential. Lowering of  $W$  by a modest factor of two or three lead to changes in back-angle scattering by several orders of magnitude. This effect was dubbed in literature improperly as incomplete absorption. This severe sensitivity of back-angle scattering to the imaginary strength of the optical potential was explained as a sudden emergence of the giant resonances of the high-partial-wave strength functions, as  $W$  decreases[6]. A more popular explanation is the interference between the wave reflected at the internal angular momentum barrier with the wave reflected at the nuclear radius.

Analysis of several heavy ion elastic scattering angular distribution in the energy range of 4-10 MeV/A conclude that backward-angle structures are caused by very few partial waves close to grazing collision value  $\ell = kR$ . Consequently, all theoretical approaches have to strengthen the contribution from these partial waves relative to the normal optical or diffraction model. Cowley and Heymann [7] and McVoy [8] parametrize the scattering amplitude by a Regge pole expansion in angular momentum. The explanation in terms of a sequence of Regge poles suggests that the physical mechanism behind the large angle structures could be heavy ion orbiting.

Orbiting could be understood simply in terms of the classical equation of motion. Let a particle  $m$  in a strong attractive potential  $V(r)$ . Then the motion is given by

$$\frac{1}{2}m\dot{r}^2 + \frac{1}{2}\frac{L^2}{mr^2} + V(r) = E \quad (55)$$

Let the effective interaction  $U(r, L) = \frac{1}{2}\frac{L^2}{mr^2} + V(r)$  and assume that for a certain angular momentum  $L = L_o$  the effective interaction has a maximum  $U_{max}$  and  $U_{max} = E$ . If this condition is satisfied then the radial velocity  $\dot{r} = 0$  and the particle is orbiting indefinitely with a radius corresponding to the maximum. For  $E$  close to the critical energy the particle remains a finite time in this state.

In this paper we reviewed the semiclassical theory of Brink and Takigawa [9] in relation with heavy ion orbiting, barrier-top resonances and Regge poles. In a second part of the paper we examine the ability of the double folding model of the optical potential to describe orbiting. In a third paper we analyze orbiting in reactions initiated by loosely bound  ${}^6\text{Li}$  at energies around 10 MeV/A, and energy range where it is believed that reactions in psd shell are peripheral and therefore it provides a favorable window for ANC applications to nuclear astrophysics. It is shown that strong refractive effects survive in such reactions and the dominant reaction mechanism is orbiting. As usual a dual interpretation is possible in terms of resonant/Regge pole description in the spirit of McVoy. See figure 43 for the most spectacular absorption profile with two active Regge poles.

## References

- [1] L. Trache, A. Azhari, H. L. Clark, C. A. Gagliardi, Y.-W. Lui, A. M. Mukhamedzhanov, R. E. Tribble, F. Carstoiu Phys. Rev. C **61**, 024612(2000).
- [2] T. Al-Abdullah, F. Carstoiu, X. Chen, H. L. Clarke, C. A. Gagliardi, Y.-W. Lui, A. Mukhamedzhanov, G. Tabacaru, Y. Takimoto, L. Trache, R.E.Tribble, Y. Zhai Phys. Rev. C **89**, 025809 ( 2014).
- [3] T. Al-Abdullah, F. Carstoiu, C. A. Gagliardi, G. Tabacaru, L. Trache and R. E. Tribble. Phys. Rev. C **89**, 064602 (2014).

- [4] G. Gaul, H. Lüdecke, R. Santo, H. Schmeing and R. Stock, Nucl. Phys. **A137**, 177 (1969).
- [5] H. Oeschler, H. Schröter, H. Fuchs, L. Baum, G. Gaul, H. Ludeke, R. Santo and R. Stock, Phys. Rev. Lett. **28**, 694 (1972).
- [6] D. M. Brink, J. Grotowski and E. Vogt, Nucl. Phys. **A309** 359(1978).
- [7] A. A. Cowley and G. Heymann, Nucl. Phys. **A146**, 465 (1970).
- [8] K. W. McVoy, Phys. Rev. C **3**, 1104 (1971).
- [9] D. M. Brink and N. Takigawa, Nucl. Phys. **A279**, 159 (1977).
- [10] W. A. Friedman and C. J. Goebel, Ann. Phys. **104**, 145 (1977).

## 7.2 Imaginary part of the ${}^9\text{C}$ - ${}^9\text{Be}$ single-folded optical potential

Single folded potentials for heavy ion reactions were proposed half a century ago and soon rejected as a useful method on the basis that the phenomenological nucleon-target potential used as a starting ingredient contains many-body correlations in an average way that lead to a nonphysical normalization  $N_V \approx 2$ . We show that it is possible to build a single-folded light nucleus- ${}^9\text{Be}$  imaginary optical potential which is more accurate than a double-folded optical potential. By comparing to experimental reaction cross sections, we showed for  ${}^8\text{B}$ ,  ${}^8\text{Li}$ , and  ${}^8\text{C}$  projectiles, that a very good agreement between theory and data could be obtained with such a bare potential, at all but the lowest energies where a small semimicroscopic surface term is added to the single-folded potential to take into account projectile breakup. In this paper we extend this study to the case of  ${}^9\text{C}$  projectiles and assess the sensitivity to the projectile density used. We then obtained the modulus of the nucleus-nucleus S matrix and parametrize it in terms of a strong-absorption radius  $R_s$  and finally extracted the phenomenological energy dependence of this radius. This approach could be the basis for a systematic study of optical potentials for light exotic nuclei scattering on light targets and/or parametrizations of the S matrix. Furthermore our study will serve to make a quantitative assessment of the description of the core-target part of knockout reactions, in particular their localization in terms of impact parameters.  ${}^9\text{Be}$  is chosen as a target in breakup reactions at intermediate energies since it behaves as a perfect black disk (it has no bound excited states) and thus the stripping component of the breakup cross section is maximized. We remind that the elastic breakup or diffraction dissociation component is more difficult to describe theoretically. Also the Coulomb dissociation is small for this target. Light exotic nuclei have been studied extensively in the last 30 years and their structure was first enlightened from measurements of the total reaction cross sections analyzed in terms of the Glauber model. This lead automatically to calculations of imaginary parts of the nucleus-nucleus optical potential in the folding model. Such a procedure, although very simple, is questionable because the folding model is first order in the nucleon-nucleon interaction, while the Feshbach imaginary potential is second order for a real nucleon-nucleon interaction.

Furthermore for light projectiles on light targets, the optical model itself has to be handled with great care. Recently we have argued that using two very successful n-<sup>9</sup>Be optical potentials and microscopic projectile densities, such as the ab initio VMC (Variational MonteCarlo), it is possible to build a single-folded light nucleus-<sup>9</sup>Be optical potential which is more accurate than a double-folded optical potential thus overcoming the difficulties discussed above. This is because the n-<sup>9</sup>Be optical potentials have strong surface terms in common for both the real and the imaginary parts which represent deformation effects, giant resonance excitations, and the breakup channels of the target. On the other hand, ab initio VMC [4,5] or other microscopic densities for the projectile would not contain enough information to reproduce the breakup channels of the projectile. By comparing to experimental reaction cross sections, we showed in Ref. [2], that for the cases of <sup>8</sup>B, <sup>8</sup>Li, and <sup>8</sup>C projectiles, a very good agreement between theory and data could be obtained by adding, at the lower energies, a small surface term to the single-folded potential. In this paper we extend the study to the case of <sup>9</sup>C projectiles, compare to results obtained with the JLM potential, and assess the sensitivity of the result to the projectile density used. We obtain then the nucleus-nucleus S matrix,  $S_{NN}$ , and parametrize  $|S_{NN}|^2$  in terms of a strong-absorption radius and finally extract the phenomenological energy dependence of the parameter  $R_s$ . Our results could have interesting implications in knockout formalisms as well. <sup>9</sup>Be is one of the ideal black-disk targets because it does not have bound excited states and for this reason it has been chosen in the majority of cases in which breakup of the projectile or total reaction cross sections have been studied. It has strong breakup channels itself but indeed these are taken into account by the n-<sup>9</sup>Be optical potentials [3] we have developed which are able to reproduce at the same time the total, elastic, reaction cross sections and all available elastic scattering angular distributions. On the other hand, one of the motivations for paying particular attention to <sup>9</sup>C as a projectile, is in nuclear astrophysics [10]: the current knowledge of the rate of the <sup>8</sup>B (p,γ) <sup>9</sup>C reaction in stellar conditions is contradictory at best and there is little hope to resolve this, now or in the future, by means other than by indirect methods such as for example the ANC from the breakup <sup>9</sup>C → <sup>8</sup>B+p. This reaction gives a possible path to the hot pp chain *pp*-IV at high temperatures and away from it toward a rapid α process at high temperatures and densities and therefore it is important in understanding nucleosynthesis in super massive hot stars in the early universe, including the possible of bypassing the 3α process. The correct description of the breakup reaction implies a precise knowledge of the various optical potentials and the corresponding S matrices at intermediate energies in the <sup>9</sup>C-target, <sup>8</sup>B-target, and p-target channels. Another motivation is two-proton radioactivity which has been studied recently by the HiRA collaboration [11-14]. They have applied nucleon removal to situations in which the remaining core is beyond the drip line, such as <sup>8</sup>C, unbound by one or more protons, and whose excitation-energy spectrum can be obtained by the invariant-mass method. By gating on the ground-state peak, core parallel-momentum distributions and total knockout cross sections have been obtained similar to previous studies with well-bound cores. In addition for each projectile, knock out to final bound states has also been obtained in several cases.

#### References

- 1 I. Tanihata, J. Phys. G. 22, 157 (1996).

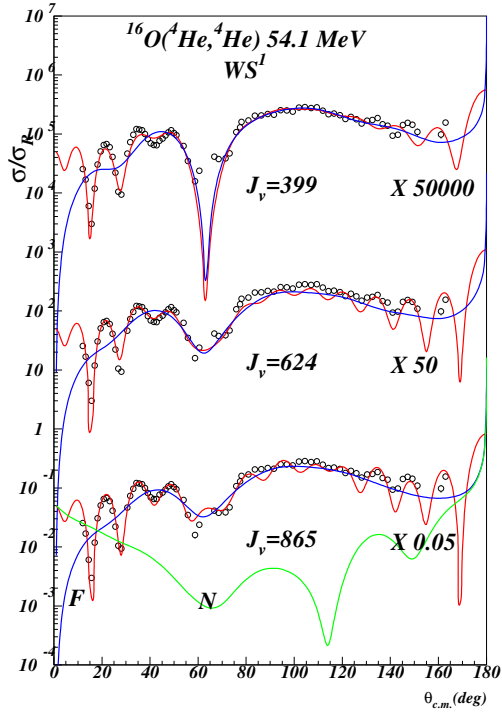


Figure 33: (Color online) F/N decomposition for the  $WS^1$  potentials.

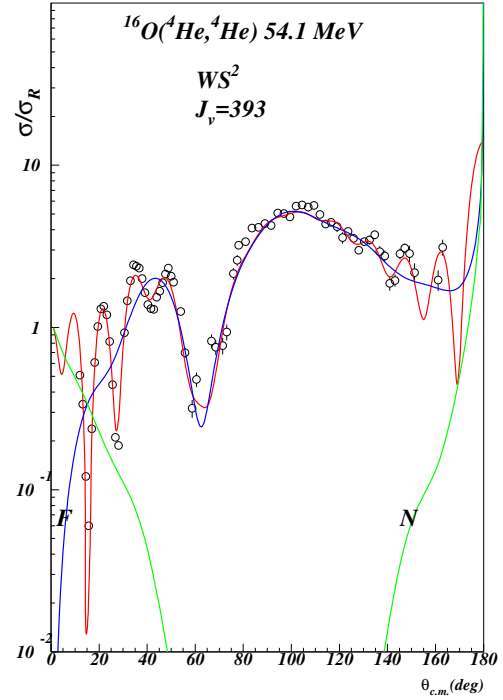


Figure 34: (Color online) F/N decomposition for the  $WS^2$  potential.

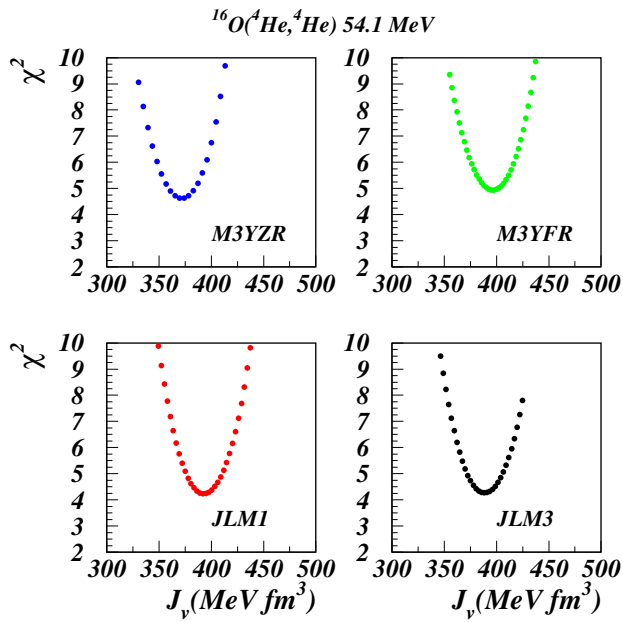


Figure 35: (Color online) Grid search with folding form factors. Unique solution.

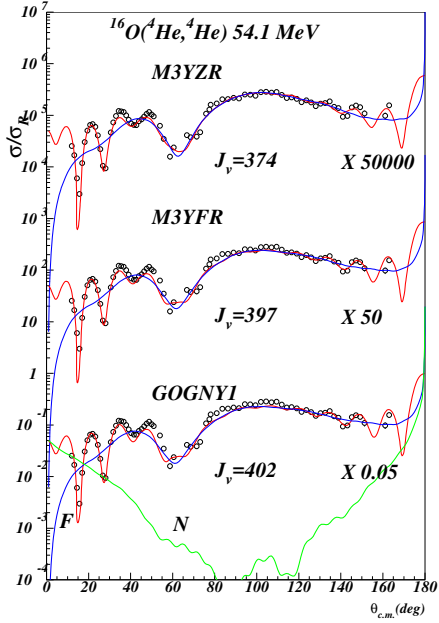


Figure 36: (Color online) F/N decomposition for the folding potentials.

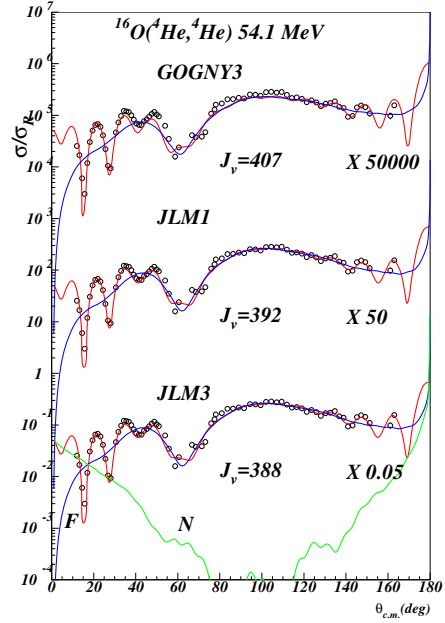


Figure 37: (Color online) F/N decomposition for the other folding potentials.

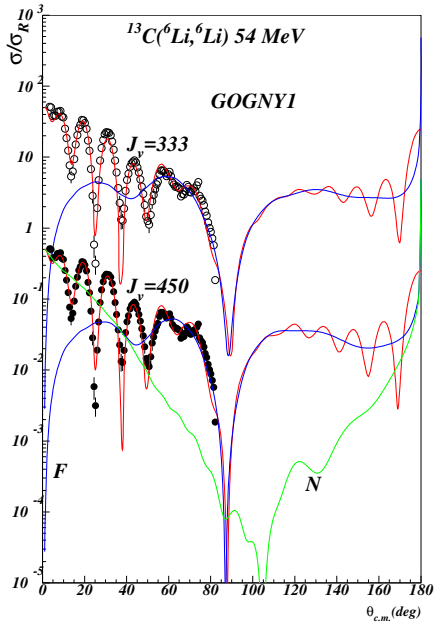


Figure 38: F/N decomposition with GOGNY1. Extremely deep Airy oscillation.

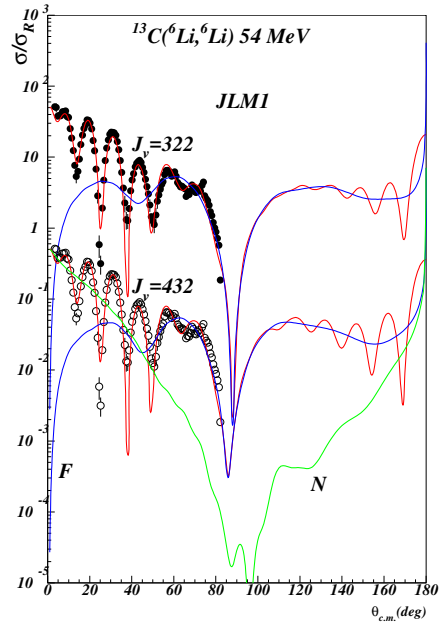


Figure 39: F/N decomposition with JLM1.

2 A. Bonaccorso, F. Carstoiu, R. J. Charity, R. Kumar, and G. Salvioni, Few-Body Syst. 57, 331 (2016).

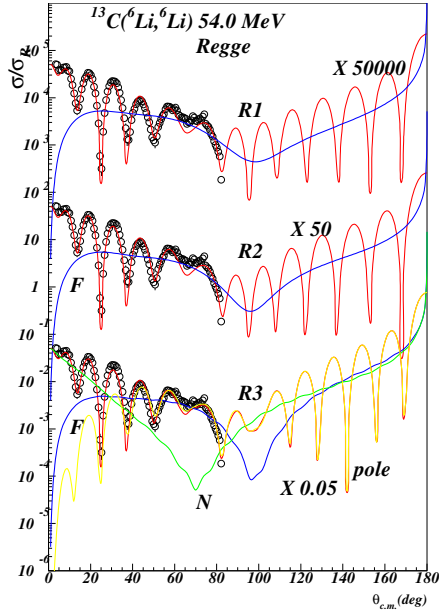


Figure 40: F/N decomposition using Regge pole amplitudes. The drop in the cross section near  $\theta = 80^\circ$  appears as a F/N interference. At large angles the dominant pole component shows a pattern similar to  $P_L^2$  with angular momentum close to the orbiting momentum  $\lambda_o = 12$ .

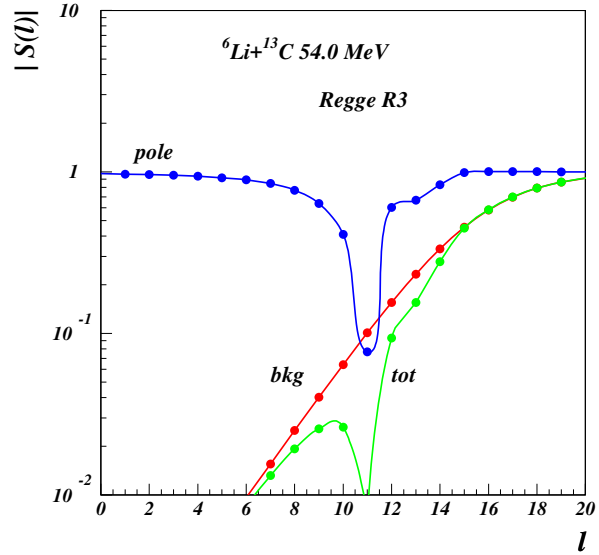


Figure 41: Absorption profile using Regge pole amplitude R3. The pole component modifies dramatically the total profile. In this case the Grünh-Wall deep is carried entirely by the pole component.

- 3 A. Bonaccorso and R. J. Charity, Phys. Rev. C 89, 024619 (2014).
- 4 R.B.Wiringa, <http://www.phy.anl.gov/theory/research/density/>.
- 5 S. C. Pieper and R. B. Wiringa, Annu. Rev. Nucl. Part. Sci. 51, 53 (2001).
- 6 J. P. Jeukenne, A. Lejeune, and C. Mahaux, Phys. Rev. C 16, 80 (1977).
- 7 F. Duggan, M. Lassaut, F. Michel, and N. Vinh Mau, Nucl. Phys. A 355, 141 (1981).
- 8 L. Trache, A. Azhari, H. L. Clark, C. A. Gagliardi, Y.-W. Lui, A. M. Mukhamedzhanov, R. E. Tribble, and F. Carstoiu, Phys. Rev. C 61, 024612 (2000).
- 9 A. Bonaccorso and F. Carstoiu, Phys. Rev. C 61, 034605 (2000).
- 10 T. Motobayashi, Nucl. Phys. A 718, 101c (2003); private communication.
- 11 R. J. Charity et al., Phys. Rev. C 84, 014320 (2011).

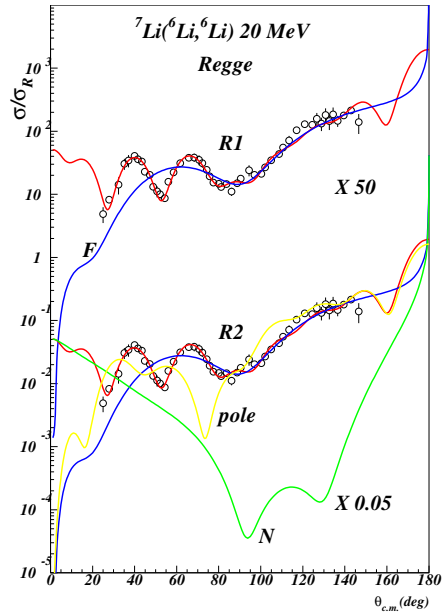


Figure 42: F/N decomposition using Regge pole amplitudes. The cross section is dominated by the pole component (yellow) in the entire angular range.

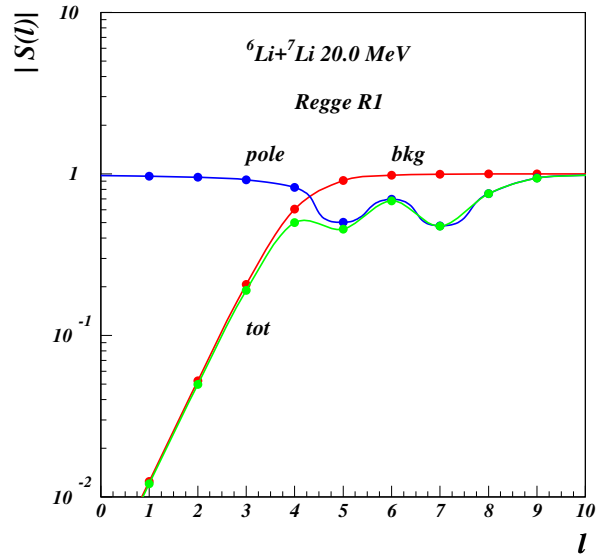


Figure 43: Absorption profile using Regge pole amplitude R1. The background component is plotted in red. There are two main poles located near the real axis  $\ell = 5$  and  $\ell = 7$ .

12 M. F. Jager et al., Phys. Rev. C 86, 011304(R) (2012).

13 I. A. Egorova et al., Phys. Rev. Lett. 109, 202502 (2012).

14 K. W. Brown et al., Phys. Rev. Lett. 113, 232501 (2014).

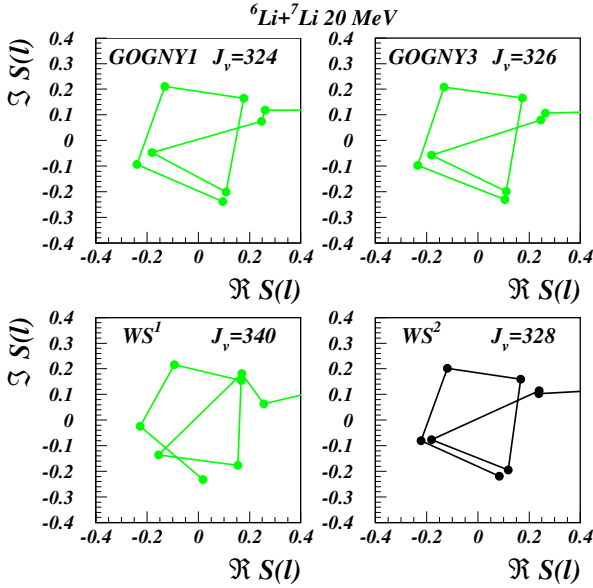


Figure 44: Comparative Argand diagram for GOGNY and WS solutions. The complex pattern arises due to the presence of two strong Regge poles (see also Fig. 43).

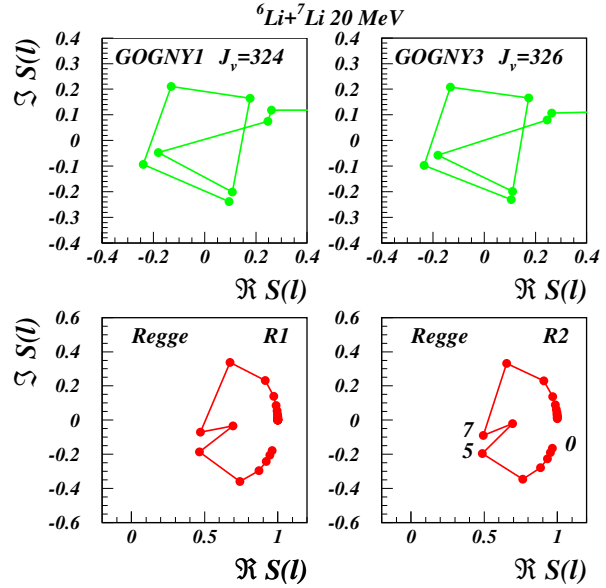


Figure 45: Comparative Argand diagrams using GOGNY solutions and Regge pole amplitudes (pole component). The numbers in the diagram indicate the angular momentum. The poles are located near  $\ell = 5$  and  $\ell = 7$ .

## 8 Published papers

### 8.1 Published papers 2011

- 1 *Bare  $\alpha$ - $\alpha$  potential and implications on  $\alpha$ -matter properties.*

INTERNATIONAL JOURNAL OF MODERN PHYSICS vol 20, No.4 (2011) 885-888 F. Carstoiu, S. Misicu, M. Rizea, M. Lassaut

Note: this paper was supported by CNCSIS, Programme PN-II-PCE- 2007-1, contracts No.49 and No.258, but not reported in the previous reports. It is reported here.

- 2 *ABSENCE OF A MAXIMUM IN THE S FACTOR AT DEEP SUB-BARRIER ENERGIES IN THE FUSION REACTION  $^{40}\text{Ca} + ^{40}\text{Ca}$ .*

Serban Misicu and Florin Carstoiu

PHYSICAL REVIEW C 84, 0501600(R) 2011

- 3 *Refractive versus resonant diffraction scattering of loosely bound nuclei*

Florin Carstoiu, Serban Misicu, Livius Trache

submitted nov 2011

to appear in:

Romanian Journal of Physics, vol. 57. No.1-2,(2012).

- 4 *Structure of  $^{23}\text{Al}$  from the one-proton breakup reaction and astrophysical implications* A. Banu, L. Trache, **F. Carstoiu**, N. L. Achouri, A. Bonaccorso, W. N. Catford, M. Chartier, M. Dimmock, B. Fernandez-Dominguez, M. Freer, L. Gaudefroy, M. Horoi, M. Labiche, B. Laurent, R. C. Lemmon, F. Negoita, N. A. Orr, S. Paschalis, N. Patterson, E. S. Paul, M. Petri, B. Pietras, B. T. Roeder, F. Rotaru, P. Roussel-Chomaz, E. Simmons, J. S. Thomas, and R. E. Tribble  
Physical Review C 84,015803,(2011)  
Note: this paper was supported by CNCSIS,Programme PN-II-PCE- 2007-1, contract No.258, but not reported in the previous reports. It is reported here.

## 8.2 Published papers 2012

- 1 *Refractive Versus Resonant Diffraction Scattering Of Loosely Bound Nuclei*  
**Florin Carstoiu**, Serban Misicu, Livius Trache  
Roum. Journ. Phys. vol.57, Nos.1-2, p. 106-137, 2012
- 2 *Direct radiative proton capture  $^{23}\text{Al}(p,\gamma)^{24}\text{Si}$  studied via one-proton nuclear breakup of  $^{24}\text{Si}$*   
A Banu,**F. Carstoiu**, W N Catford, B Fernandez-Dominguez, M Horoi, N A Orr, B T Roeder, P Roussel-Chomaz, L Trache and R E Tribble  
Nuclear Physics in Astrophysics V  
Journal of Physics:Conference Series 337 (2012) 012059
- 3 *One proton breakup of  $^{24}\text{Si}$  and the  $^{23}\text{Al}(p,\gamma)^{24}\text{Si}$  reaction in type I x-ray bursts.*  
A. Banu, **F. Carstoiu**, N. L. Acouri, W. N. Catford, M. Chartier, B. Fernandez-Dominguez, M. Horoi, B. Laurent, N. A. Orr, S. Paschalis, N. Patterson, B. Pietras, B. T. Roederer, P. Roussel-Chomaz, J. S. Thomas, L. Trache, and R. E. Tribble  
Physical Review C86, 015806(2012).
- 4 *Erratum:One proton breakup of  $^{24}\text{Si}$  and the  $^{23}\text{Al}(p,\gamma)^{24}\text{Si}$  reaction in type I x-ray bursts.*  
A. Banu, **F. Carstoiu**, N. L. Acouri, W. N. Catford, M. Chartier, B. Fernandez-Dominguez, M. Horoi, B. Laurent, N. A. Orr, S. Paschalis, N. Patterson, B. Pietras, B. T. Roederer, P. Roussel-Chomaz, J. S. Thomas, L. Trache, and R. E. Tribble  
Physical Review C86, 039901(E)(2012)

5 *Refractive versus resonant diffraction scattering of loosely bound  ${}^6\text{Li}$  nuclei*

**Florin Carstoiu** and Livius Trache

PHYSICAL REVIEW C 85, 054606 (2012)

6 *A convenient coordinatization of Siegel Jacobi domains*

**Stefan Berceanu**

Reviews in Mathematical Physics

Vol. 24, No. 10 (2012) 1250024 (38 pages) World Scientific Publishing Company DOI:  
10.1142/S0129055X12500249

7 *Alpha-decay data of superheavy nuclei as a source of information about nuclear states*

**I. SILISTEANU, A. I. BUDACA**

Roum. Journ. Phys. vol. 57, Nos.1-2, p. 403-505

### 8.3 Published papers 2013

1 *Alpha-decay data of superheavy nuclei as a source of information about nuclear states*

I. SILISTEANU, A. I. BUDACA

Roum. Journ. Phys. vol. 57, Nos.1-2, p. 403-505

2 *Low-energy  $\alpha - \alpha$  semimicroscopic potentials*

M. LASSAUT, F. CARSTOIU, V. BALANICA

Roum. Journ. Phys. vol. 57, Nos.7-8, p. 913-930

3 *A useful parametrization of Siegel-Jacobi manifolds*

S. BERCEANU

PROCEEDINGS OF THE XXX WORKSHOP ON GEOMETRIC METHODS IN PHYSICS,

P. Kielanowski, S. Twareque Ali, A. Odesski, A. Odziejewicz, M. Schlichenmaier and T.  
Voronov, editors,

Trends in Mathematics, Birkhauser, Springer Basel AG 99–108, 2013.

4 *Dynamical scission model*

M. RIZEA, N. CARJAN

Nucl.Phys.A909(2013)p.50-68

### 8.4 Published papers in 2014

1 Stefan Berceanu, *Coherent states and geometry on the Siegel-Jacobi disk*, INT. J. GEOM.

METHODS MOD. PHYS. published on February 13 2014, DOI: 10.1142/S0219887814500352,

Print ISSN: 0219-8878, Online ISSN: 1793-6977

- 2 *Astrophysical reaction rate for  $^{17}\text{F}(p,\gamma)^{18}\text{Ne}$  from the transfer reaction  $^{13}\text{C}(^{17}\text{O},^{18}\text{O})^{12}\text{C}$*   
T.Al-Abdullah, F. Carstoiu, X. Chen, H.L. Clarke, C.A. Cagliardi, Y.-W. Lui, A. Mukhamedzhanov, G. Tabacaru, Y. Takimoto, L. Trache, R.E.Tribble, Y. Zhai PHYS. REV. C 89, 025809 (2014)
- 3 *Determination of the asymptotic normalization coefficients for  $^{14}\text{C} + n \leftrightarrow ^{15}\text{C}$ , the  $^{14}\text{C}(n,\gamma)^{15}\text{C}$  reaction rate, and evaluation of a new method to determine spectroscopic factors*, M. McCleskey, A. M. Mukhamedzhanov, L. Trache, R. E. Tribble, A. Banu, V. Eremenko, V. Z. Goldberg, Y.-W. Lui, E. McCleskey, B. T. Roeder, A. Spiridon, F. Carstoiu, V. Burjan, Z. Hons and I. J. Thompson, PHYSICAL REVIEW C 89, 044605 (2014)
- 4 *Peripheral elastic and inelastic scattering of  $^{17,18}\text{O}$  on light targets at 12 MeV/nucleon*, T. Al-Abdullah, F. Carstoiu, C.A. Gagliardi, G. Tabacaru, L. Trache and R.E. Tribble. PHYSICAL REVIEW C 89, 064602 (2014).
- 5 S. Berceanu, *Quantum mechanics and geometry on Siegel-Jacobi disk*, talk at XXXII workshop of Geometric Methods in Physics, -Bialowieza, 29 June- 6 July 2013, published on July-15, ISBN 978-3-319-06248-8, Birkhauser Basel(2014)

## 8.5 Published papers in 2015

- 1 Peripheral elastic and inelastic scattering of  $^{17,18}\text{O}$  on light targets at 12 MeV/nucleon  
F. Carstoiu, T. Al-Abdullah, C. A. Gagliardi and L. Trache  
AIP Conference proceedings, vol 16454, p39 (2015)  
Carpathian Summer School of Physics, Sinaia, 13-26 July, 2014
- 2 S. Berceanu; Wei-Norman and Berezin's equations of motion on the Siegel-Jacobi disk  
Rom. J. Phys., Vol.60, fasc.1-2, p.126-146, 2015.  
S. Berceanu
- 3 Bergman representative coordinates on the Siegel-Jacobi Disk  
Rom. J. Phys., Vol.60, fasc.7-8, p. 867-896, 2015.
- 4 S. Berceanu, On equations of motion on Siegel-Jacobi spaces generated by linear Hamiltonians in the generators of the Jacobi group, talk at XXX International Colloquium on Group Theoretical Methods in Physics, 14 July-18 July 2014, Ghent, Belgium 2015 J. Phys.: Conf. Ser. 597 012016

## 8.6 Published papers 2016

- 1 Heavy Ion Orbiting and Regge Poles (I), **F. Carstoiu**, M. Lassaut. L. Trache, **V. Balanica**, ROMANIAN JOURNAL OF PHYSICS, Vol. 61, Nos. 3-4, P.400-412, 2016.

- 2 Heavy Ion Orbiting and Regge Poles (II), **F. Carstoiu**, M. Lassaut. L. Trache, **V. Balanica**, ROMANIAN JOURNAL OF PHYSICS, Vol. 61, Nos. 5-6, P.857-874, 2016.
- 3 A. Bonaccorso, **F. Carstoiu**, R. J. Charity, R. Kumar, Differences Between a Single- and Double-Folding Nucleus- $^9\text{Be}$  Optical Potential, Few Body Syst., Vol. 57, No. 5, p. 331-336, DOI 10.1007/s00601-016-1082-4, 2016.
- 4 **S. Berceanu**, Balanced Metric and Berezin Quantization on the Siegel-Jacobi Ball, Symmetry, Integrability and Geometry: Methods and Applications, SIGMA 12, 064, 28 pages, <http://dx.doi.org/10.3842/SIGMA.2016.064>, 2016.
- 5 A. Bonaccorso, **F. Carstoiu**, and R. J. Charity, Imaginary part of the  $^9\text{C}$ - $^9\text{Be}$  single-folded optical potential, PHYSICAL REVIEW C 94, 034604 (2016), DOI: 10.1103/PhysRevC.94.034604
- 6 **S. Berceanu**, Geodesics Associated to the Balanced Metric on the Siegel-Jacobi Ball, ROMANIAN JOURNAL OF PHYSICS, Vol. 61, Nos. 7-8,p. 1137-1160, 2016
- 7 Heavy Ion Orbiting and Regge Poles (III), **F. Carstoiu**, M. Lassaut. L. Trache, **V. Balanica**, ROMANIAN JOURNAL OF PHYSICS, Vol. 61, Nos. 7-8,p. 1180-1197, 2016

PROJECT DIRECTOR: dr. F. Carstoiu